© 2020. Published by The Company of Biologists Ltd | Development (2020) 147, dev188714. doi:10.1242/dev.188714

RESEARCH ARTICLE

Nuclear-encoded mitochondrial ribosomal proteins are required to initiate gastrulation

Agnes Cheong, Danielle Archambault, Rinat Degani, Elizabeth Iverson, Kimberly D. Tremblay and Jesse Mager*

ABSTRACT

Mitochondria are essential for energy production and although they have their own genome, many nuclear-encoded mitochondrial ribosomal proteins (MRPs) are required for proper function of the organelle. Although mutations in MRPs have been associated with human diseases, little is known about their role during development. Presented here are the null phenotypes for 21 nuclear-encoded mitochondrial proteins and in-depth characterization of mouse embryos mutant for the Mrp genes *Mrpl3*, *Mrpl22*, *Mrpl44*, *Mrps18c* and *Mrps22*. Loss of each MRP results in successful implantation and egg-cylinder formation, followed by severe developmental delay and failure to initiate gastrulation by embryonic day 7.5. The robust and similar single knockout phenotypes are somewhat surprising given there are over 70 MRPs and suggest little functional redundancy. Metabolic analysis reveals that Mrp knockout embryos produce significantly less ATP than controls, indicating compromised mitochondrial function. Histological and immunofluorescence analyses indicate abnormal organelle morphology and stalling at the G2/M checkpoint in Mrp null cells. The nearly identical pre-gastrulation phenotype observed for many different nuclear-encoded mitochondrial protein knockouts hints that distinct energy systems are crucial at specific time points during mammalian development.

This article has an associated 'The people behind the papers' interview.

KEY WORDS: MRP, *Bcs1l*, *Clpx*, *Fastkd5*, *Hlcs*, *Isca1*, *Mars2*, *Mrpl3*, *Mrpl22*, *Mrpl44*, *Mrps18c*, *Mrps22*, *Mrps25*, *Mtpap*, *Nars2*, *Ndufa9*, *Ndufs8*, *Pmpcb*, *Sdhaf2*, *Timm22*, *Trit1*, *Tomm20*, Mitochondria, Mouse embryo, Gastrulation

INTRODUCTION

Mitochondria are membrane-bound organelles that participate in energy production and diverse cellular functions including calcium signaling, redox homeostasis and apoptosis (Chandel, 2015; Tait and Green, 2012). Among their many functional roles, mitochondria are widely regarded as the 'powerhouse' of eukaryotic cells (Fu et al., 2019; De Silva et al., 2015; Lee and Han, 2017; Tait and Green, 2012). In the presence of oxygen, ATP is generated via the electron transport chain (ETC) located in the inner mitochondrial membrane, a process that is known as oxidative phosphorylation (OXPHOS) (Lee and Han, 2017). Distinct from other eukaryotic organelles, mitochondria encapsulate their own genomic DNA, which is transcribed and translated within the organelle (Lee and Han, 2017). The mitochondrial genome is ∼16.5 kbp in size (16,569 bp in humans and 16,295 bp in mice) and encodes 2 ribosomal RNAs (rRNA) and 22 transfer RNAs (tRNA) as well as 13 proteins that are indispensable for the ETC (Lee and Han, 2017). The mitochondrial transcription and translation machinery is entirely encoded by genes in the nuclear genome that are imported into the mitochondria after cytosolic protein synthesis (Boengler et al., 2011).

In response to cellular or environmental stimuli, energetic needs can be matched via mitochondrial biogenesis, the process of increasing mitochondrial mass (Jornayvaz and Shulman, 2010). Mitochondria also require regular maintenance, which is accomplished by undergoing fusion and fission, allowing the mitochondrial network to repair and reorganize. To accommodate for high energy demands required by events such as cell proliferation and differentiation, mitochondria fuse together to increase OXPHOS (Fu et al., 2019; Yao et al., 2019). Fusion events can also promote mitochondrial complementation, a process that allows mutated mitochondrial DNA (mtDNA) to be compensated by wild-type mtDNA (Youle and van der Bliek, 2012). During cell division, mitochondria are partitioned via fission, allowing a subset of mitochondria to be delivered to each daughter cell (Mishra and Chan, 2014).

As a double membrane bound organelle, mitochondria contain an outer mitochondrial membrane encapsulating an inner mitochondrial membrane that separates the matrix and the intermembrane space. Within the matrix, the electron carriers NADH and $FADH_2$, generated from the Krebs cycle transfer their electrons to the ETC, located in the inner mitochondrial membrane (Lodish et al., 2000). As the electron is transferred across the protein complexes, protons are pumped from the matrix to the intermembrane space, generating a proton gradient. This gradient subsequently drives protons through the ATP synthase, resulting in the synthesis of ATP in the matrix. Utilizing the mitochondrial ADP/ATP carrier, ATP is exported into the intermembrane space and released from the mitochondria via channels such as the voltage-dependent anion channel (VDAC), which is abundant in the outer mitochondrial membrane (Camara et al., 2017; Kunji et al., 2016; Lodish et al., 2000).

Mitochondrial function is essential for embryogenesis – a process that involves rapid cell growth and movement. Previous knockout mouse models have shown that mutations in the genes required for mitochondrial maintenance and biogenesis result in lethality during mid and late gestation (Baker and Ebert, 2013; Humble et al., 2013; Wakabayashi et al., 2009; Chen et al., 2003; Barak et al., 1999). Additionally, mitochondria have been shown to play a crucial role before fertilization as knockout of mitoguardin genes (*Miga1* and *Miga2*) negatively impacts ovulation (Liu et al., 2017).

Prior to fertilization, mitochondria in the oocyte are round with few cristae (Zhang et al., 2017; Lima et al., 2018). The oocyte is

Department of Veterinary and Animal Sciences, University of Massachusetts, Amherst, MA 01003, USA.

*Author for correspondence (jmager@vasci.umass.edu)

J.M., 0000-0002-4123-0633

Handling Editor: Liz Robertson
Received 27 January 2020; Accepted 30 March 2020

Development (2020) 147, dev188714. doi:10.1242/dev.188714

quiescent with low ATP production, thus minimizing the number of mitochondrial DNA mutations (Babayev and Seli, 2015). Following fertilization, any paternal mtDNA arriving from the sperm is eliminated via mitophagy (Rojansky et al., 2016). In post-implantation embryos, the maternal mitochondria undergo structural changes that include elongation and the formation of organized cristae, presumably in response to the increased energy demands of cellular differentiation and development (Schatten et al., 2014; Prigione et al., 2015; Lima et al., 2018).

Immediately prior to and during the cleavage stages, from the one-cell zygote through the 16-cell morula, energy continues to be generated via OXPHOS (Kaneko, 2016). Concurrent with the first cell lineage decision at the blastocyst stage, energy sources within the specific cell types begin to shift. The inner cell mass (ICM) of the blastocyst, which gives rise to the embryo proper and some extraembryonic tissues, utilizes glycolysis as the primary energy source whereas the trophectoderm (TE), which contributes only to the extraembryonic tissue, predominantly utilizes OXPHOS (Kaneko, 2016). After blastocyst implantation (at embryonic day (E) 4.5 in the mouse), the E5.5 embryo forms a radially symmetric egg cylinder. By E6.5, the embryo initiates gastrulation, a dynamic morphogenetic process resulting in the emergence and reorganization of the primary germ layers (endoderm, mesoderm and ectoderm). The initiation of gastrulation results in the formation of the primitive streak, an embryonic organizing center on the posterior side of the embryo, which utilizes an epithelial-to-mesenchymal transition to specify the emerging germ layers (Downs, 2009).

Gastrulation is the first in a series of developmental events during which embryonic cells rapidly divide and initiate cellular, molecular and epigenetic differentiation programs. Given the pace and magnitude of the differentiation that occurs during this developmental transition, it is not surprising that there is a requirement for proper mitochondrial function during development (Hance et al., 2005; Humble et al., 2013; Larsson et al., 1998; Li et al., 2000; Nonn et al., 2003; Baker and Ebert, 2013; Chen et al., 2003; Bushdid et al., 2003; Qian et al., 2003; Conrad et al., 2004; Davies et al., 2007). Multiple studies provide convincing evidence that the developing embryo is reliant on the OXPHOS system for developmental progression. These studies highlight the requirement of both energy systems, glycolysis and OXPHOS, in the developing embryo. However, the lineage- and temporal-specific requirements of glycolysis and OXPHOS remain unknown. Interestingly, work in *Drosophila* has also shown that mitochondria are important in modulating the dynamic change in cell shape during gastrulation (Ratnaparkhi, 2013).

As stated above, the majority of proteins present in the mitochondria are encoded by genes in the nucleus that are imported into the mitochondria after translation. One large group of these is the mitochondrial ribosomal proteins (MRPs), of which there are more than 70 members in mammals (O'Brien et al., 2000; Bogenhagen et al., 2018). The MRP group consists of two subgroups: the mitochondrial large subunit protein (MRPL) and mitochondrial small subunit protein (MRPS). Specifically, the MRP group is composed of 48 MRPL and 30 MRPS in humans and 50 Mrpl and 29 Mrps in mice (Yates et al., 2017; Bult et al., 2019). The N terminus of most MRPs contains a transit peptide sequence that enables the translocase of mitochondrial membrane (TOM) complex to shuttle the proteins across the mitochondrial membrane (Garg et al., 2015). Once in the matrix, the MRPL and MRPS assemble with the 16S and 12S rRNA, respectively, and other mitochondrial ribosomal components to form the mitochondrial ribosome complex. This large mitoribosome complex is essential for translating proteins encoded in the mitochondrial genome and is therefore crucial for ETC function (De Silva et al., 2015).

Because MRPs are essential components of the mitochondrial translation machinery, mutations in Mrp genes are detrimental to the OXPHOS system and associated with several related human disorders (De Silva et al., 2015). For example, human *MRPL3* mutations are associated with combined oxidative phosphorylation deficiency (COXPD) 9, a *MRPL44* mutation is linked to COXPD16, and *MRPS22* is associated with cardiomyopathy (De Silva et al., 2015; Dickinson et al., 2017). Although some clinical studies have revealed the consequences of MRP abrogation in humans, little is known about the role of MRPs during mammalian embryogenesis.

Presented here are 21 novel knockout phenotypes of nuclear encoded mitochondrial proteins and detailed characterization of five Mrp phenotypes: *Mrpl3*, *Mrpl22*, *Mrpl44*, *Mrps18c* and *Mrps22*. Homozygous knockout of any one of these genes individually results in embryos that proceed through early preimplantation stages, implant and form a radially symmetric egg cylinder but fail to initiate gastrulation. Each individual knockout displays aberrant mitochondrial morphology but no apparent change in mitochondrial genome content or excessive oxidative stress. Additionally, the data indicate an alteration in ADP/ATP ratios implying that ATP production in the knockout embryos is greatly reduced. Together, these data suggest that although mitochondrial biogenesis is unaffected, mitochondrial function is compromised, resulting in reduced energy production and cell cycle perturbation in knockout embryos.

RESULTS

Mrp genes are essential for initiation of gastrulation

To explore the role of Mrp genes during embryogenesis in mice, the Mrp loss of function phenotypes were first examined. The Mrp knockout alleles were produced by the Jackson Laboratories as part of the Knockout Mouse Project (KOMP) (Dickinson et al., 2017). These knockout alleles were generated either by replacing part of the genomic locus with a *lacZ* reporter gene or by utilizing CRISPR-Cas to create deletions in coding exons (Fig. 1A). The overall morphology and developmental progress of homozygous knockout embryos were assessed by crossing heterozygous males and females for each Mrp gene (herein collectively referred to as 'mutants', 'mutant embryos' or '−/−'). At E7.5, homozygous mutants for each gene knockout were recovered at expected mendelian ratios but were significantly smaller and delayed compared with littermates (Fig. 1B). Interestingly, the mutant embryos all had a very similar phenotype across the five different Mrp knockout lines. Regardless of the Mrp that was disrupted, each mutant appeared to be stalled at approximately the size of normal E6.0 embryos, just prior to the onset of gastrulation. Furthermore, at E7.5, none of the mutants had structures typical of gastrulation: there were no morphologically evident primitive streaks, nodes, headfolds or allantois in any mutants. It is important to note that none of the mutant embryos appeared disorganized nor were there apparent pyknotic/dying cells; all of the mutants appeared as relatively pristine early egg-cylinder stage embryos at E7.5. These results suggest that development proceeded normally until E5.5-E6.0 in each knockout and then stalled, failing to progress further. At E8.5, decidua with embryo resorptions could be dissected from heterozygous intercrosses for each of the Mrp knockout alleles indicating that the failure of developmental progression eventually results in lethality and resorption.

Development (2020) 147, dev188714. doi:10.1242/dev.188714

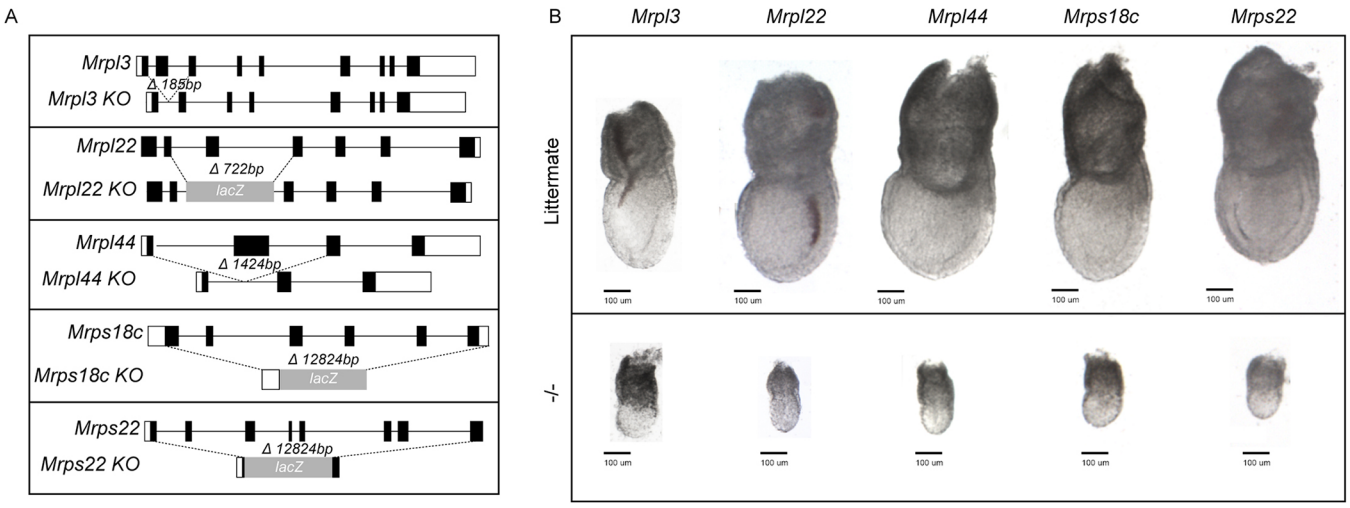

Fig. 1. Mrp null embryos are severely delayed at E7.5. (A) Design/strategy of Mrp knockout (KO) alleles. (B) Representative embryos dissected at E7.5. The upper panel shows littermate and the lower panel shows each null mutant. Mutants are dramatically smaller in size with no evident morphological hallmarks of gastrulation. Scale bars: 100 µm.

Expression analysis of each Mrp

Next, the expression of Mrp genes was assessed in various tissues and embryonic stages. Reverse transcription polymerase chain reaction (RT-PCR) using gene-specific intron-spanning primers was performed with oocytes and embryos from various stages of development (preimplantation, gastrulation and the onset of organogenesis). As shown in Fig. 2, *Mrpl3*, *Mrpl22*, *Mrpl44*, *Mrps18c* and *Mrps22* were abundantly expressed during both pre-implantation and post-implantation stages. One notable exception was the apparent epiblast specificity of *Mrps22*, which was nearly absent in the E6.5 visceral endoderm. Further examination was done to determine whether the widespread expression continued in adult tissues. The result revealed the ubiquitous expression of these Mrp genes in all adult tissues examined (Fig. 2B).

The spatiotemporal expression of *Mrpl22*, *Mrps18c*, and *Mrps22* was also examined using whole mount *in situ* hybridization or the *lacZ* reporter at various embryonic stages (Fig. 2C). Consistent with the RT-PCR results, widespread expression of the *lacZ* reporter in *Mrpl22* and *Mrps18c* was observed in heterozygous embryos from E6.5 to E9.5 (Fig. 2C). Similarly, an ISH probe specific for *Mrps22* confirmed a higher level of expression at E6.5 epiblast and embryo-specific expression in later stages (E7.5 to E9.5; Fig. 2C).

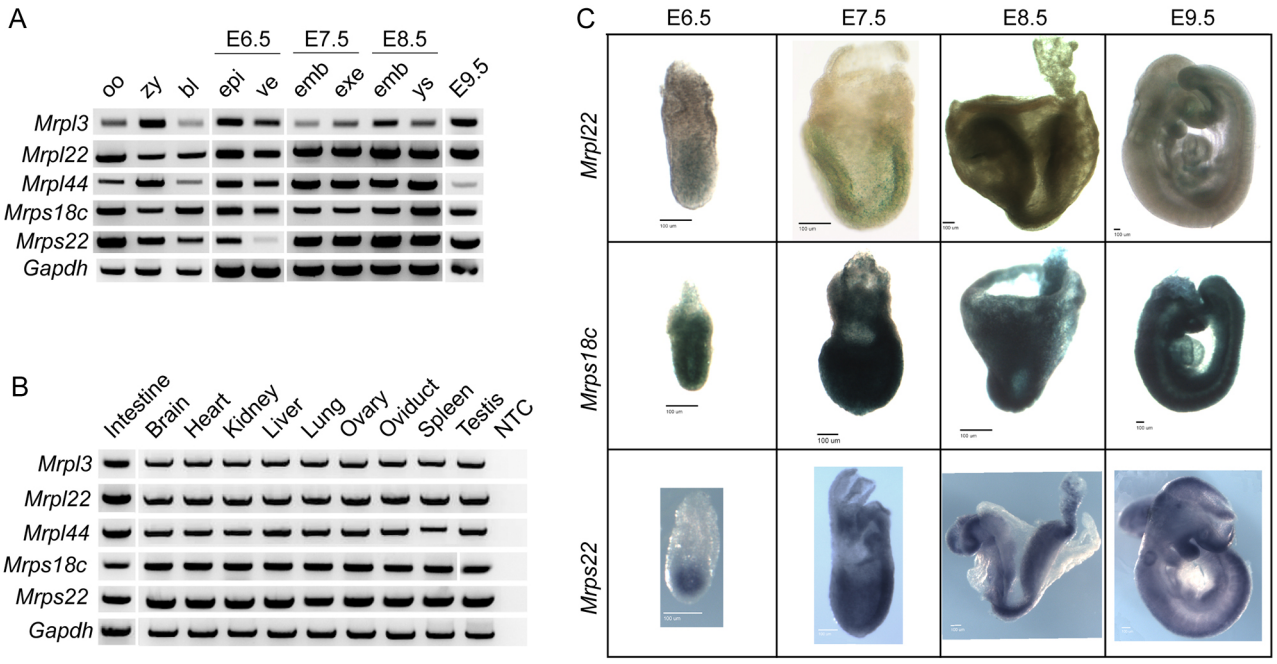

Fig. 2. Mrp genes are widely expressed in embryos and adult tissues. (A,B) RT-PCR indicates little tissue- or temporal-specific expression in all stages and tissues examined with one notable exception: *Mrps22* is nearly absent in the visceral endoderm. *Gapdh* was used as control. (C) Widespread expression was confirmed by X-gal staining in heterozygous *Mrpl22* and *Mrps18c* embryos. Epiblast-specific *Mrps22* expression was confirmed by whole mount *in situ* hybridization. oo, oocyte; zy, zygote; bl, blastocyst; epi, epiblast; ve, visceral endoderm; emb, embryonic region; exe, extraembryonic region; ys, yolk sac; NTC, no template control. Scale bars: 100 µm.

Development (2020) 147, dev188714. doi:10.1242/dev.188714

Mrp mutant embryos fail to initiate gastrulation

Because the morphological analysis suggested that null embryos from each Mrp allele arrested prior to gastrulation, these embryos were assessed for molecular markers of the primitive streak. Immunofluorescence (IF) was performed to detect the primitive streak marker Brachyury (T), the epiblast marker Oct4 and a marker of epithelial-cell membranes E-cadherin (Ecad). In normal embryos, Oct4 is expressed in the ICM of the blastocyst and this expression is retained in the pluripotent epiblast of pre-streak stage embryos. During gastrulation, Oct4 expression is reduced as cells delaminate and undergo the epithelial to mesenchymal transition required for primitive streak formation and then lost as differentiation occurs. By E7.5, Oct4-positive cells are confined to the primitive streak, primordial germ cells and prospective neuroectoderm (Schöler et al., 1990). As shown in Fig. 3, section analysis revealed that the overall organization of E7.5 mutant embryos remained the same as that of normal ∼E6.0 embryos – only two cell layers with bilaterally symmetric egg-cylinder morphology. IF revealed that cells of the epiblast in all mutants still contained robust nuclear Oct4, indicating that the pluripotent epiblast cells remained in mutants at E7.5 (Fig. 3C′-F′). In normal embryos, induction of the primitive streak via epithelial to mesenchymal transition at the posterior end of the embryo mark the onset of gastrulation at ∼E6.5 in mice. During this process, brachyury (T), a key transcription factor involved in mesoderm formation, is expressed in the node and the primitive streak of E6.5-E8.5 embryos. Following gastrulation, T expression is restricted to the notochord of the developing embryo (Wilkinson et al., 1990; Herrmann et al., 1990). As expected, T-positive cells were confined to the primitive streak and nascent mesoderm in littermates (Fig. 3A‴); however, T was not observed in any Mrp null mutants (compare Fig. 3A‴ with Fig. 3C‴-F‴). These data support the hypothesis that E7.5 mutant embryos have not progressed beyond pre-streak stages and demonstrate that loss of function of any one of these five Mrp genes results in developmental arrest and failure to initiate gastrulation.

Next, active Trp53 (a marker of apoptosis) as well as histone H3 phosphorylated at serine 10 (pH3, a marker of dividing cells) were examined to determine whether cells were dying and/or failing to proliferate in homozygous mutants. Although there were a few active Trp53-positive cells in *Mrpl22*, *Mrpl44* and *Mrps18c* mutants, widespread apoptotic cells were not observed in any of the homozygous mutants (Fig. 4A″-G″). The lack of apoptosis is consistent with the overall pristine morphology, despite the obvious developmental delay at E7.5. Normal embryos undergo rapid and widespread proliferation during gastrulation (see wild-type controls in Fig. 4) (Mac Auley et al., 1993; Snow, 1977). In proliferating cells, chromatin condenses extensively in preparation for mitosis and chromosome segregation (O'Connor, 2008). Phosphorylation of histone H3 (S10) has been highly correlated with chromatin condensation prior to mitosis and is known to have a dual role in mitosis and interphase (Hendzel et al., 1997; Wei et al., 1998; Goto et al., 2002; Li et al., 2005). Although further quantification is necessary, there appears to be increased numbers of bright pH3 foci in mutant sections compared with controls, suggesting mutant cells arrested in the G2/late G2 phase (comparing Fig. 4H″ with Fig. 4I″-M″). The lack of widespread active Trp53 combined with the severe developmental delay suggests that Mrp homozygous mutant embryos are stalled prior to gastrulation but are not dying at E7.5.

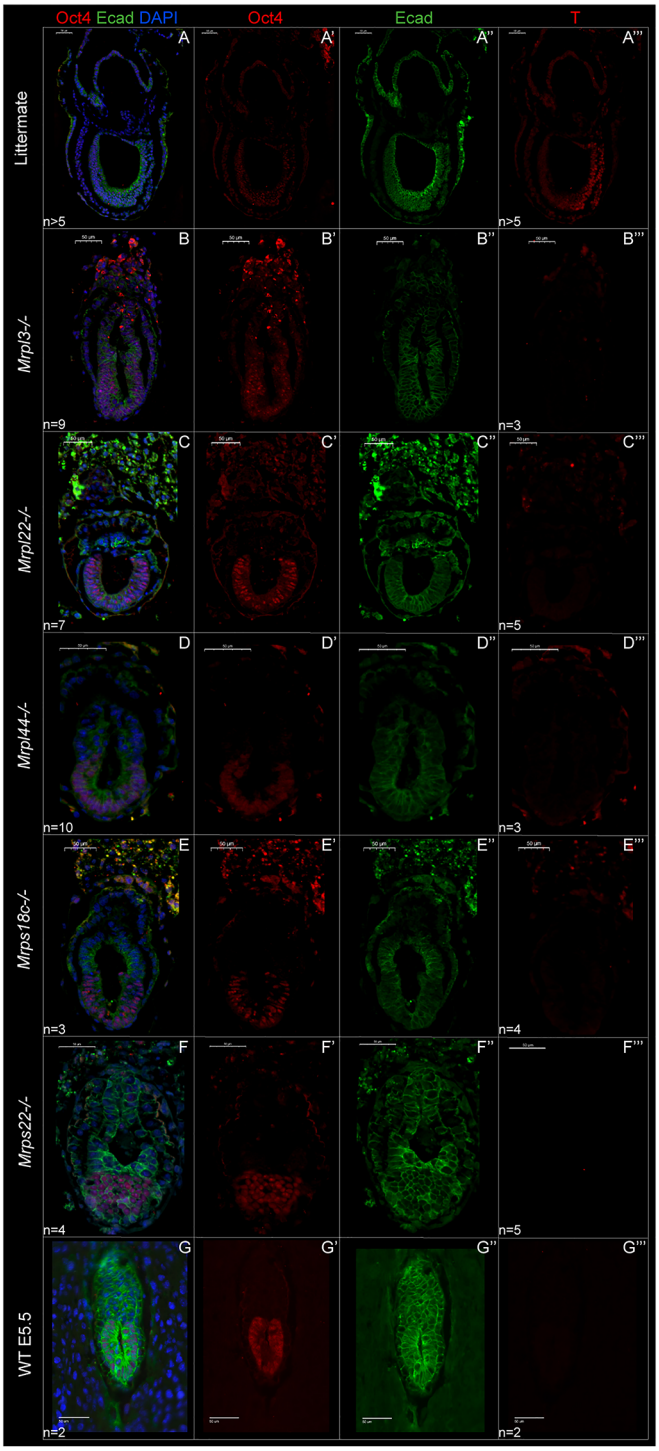

Fig. 3. Mrp null embryos fail to initiate gastrulation. (A-G) E7.5 immunofluorescence labeling of Oct4 (red), e-cadherin (green) and sequentially of brachyury (T, red) and DAPI nuclear stain (blue). (A-A‴) As expected, littermate E7.5 embryos are largely devoid of Oct4 signal, with cells of the primitive streak being T positive. (B-F) Mutant embryos retain robust Oct4 in the epiblast and no T-positive cells are evident, similar to early egg-cylinder E5.5 stage embryos (G), indicating that mutants have failed to initiate gastrulation. Note that sequential rounds of IF allow the same embryo sections to be labeled with both Oct4 and T. Scale bars: 50 µm.

Mrp genes are essential for proper mitochondrial structure and function

Because Mrp genes are thought to play essential roles in assembling the mitochondrial translation machinery, and because defects in translation can negatively impact the OXPHOS system, it is speculated that Mrp mutant embryos undergo increased oxidative stress. Elevation in reactive oxygen species (ROS) results in

Development (2020) 147, dev188714. doi:10.1242/dev.188714

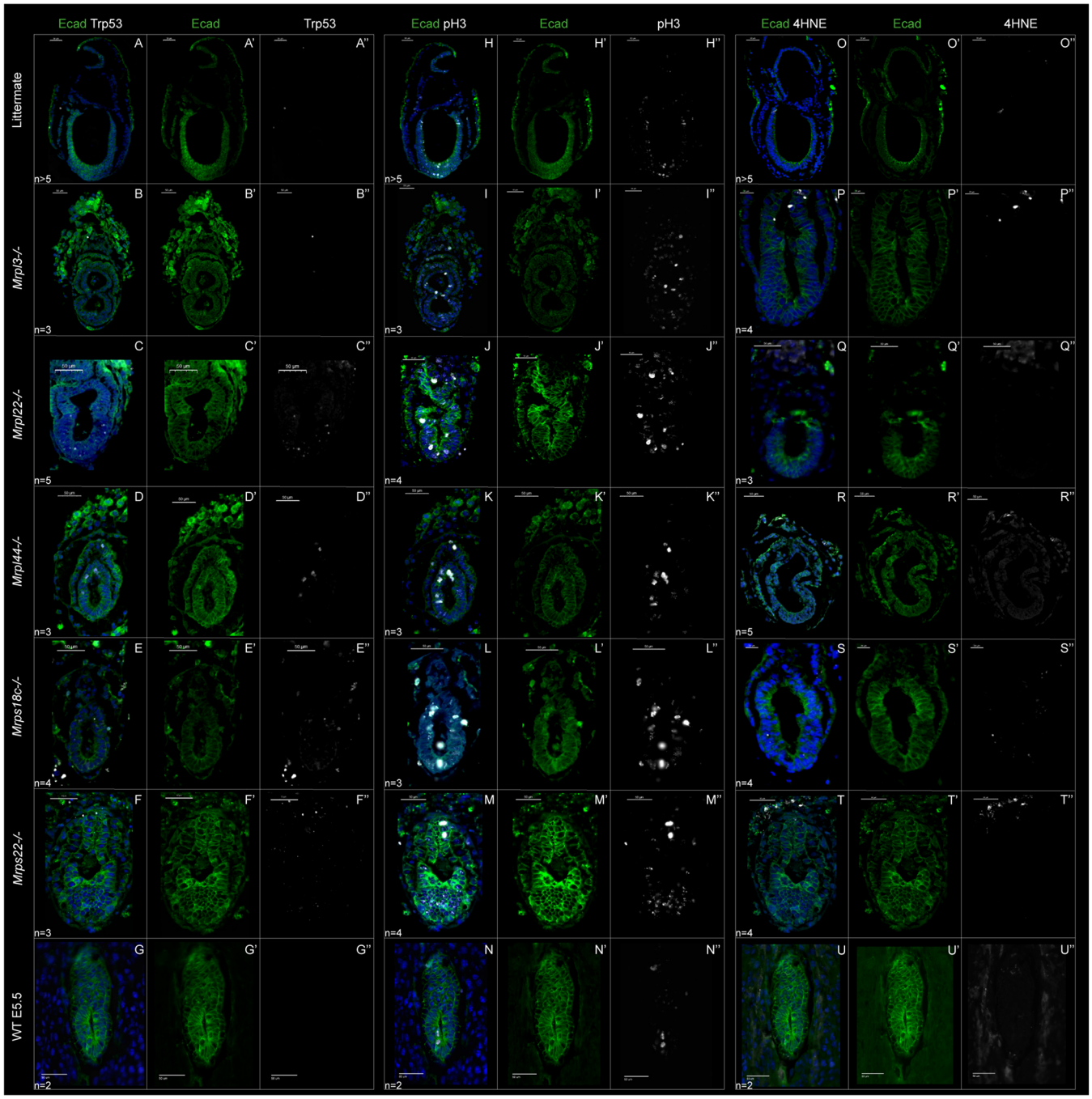

Fig. 4. Mrp null embryos do not experience excessive cell death and oxidative stress. (A-N) Embryo sections were labeled with antibodies to detect active-Trp53 (white), e-cadherin (green), and sequentially with e-cadherin (green) and pH3 (white). Similar to E7.5 littermates (A,H) and egg-cylinder stage E5.5 embryos (G,N), mutants showed widespread pH3-positive cells with minor cell death. (O-U) Embryos were labeled with 4HNE (white) and e-cadherin (green). Nuclei were counterstained with DAPI (blue). Additionally, no excessive 4HNE is observed in mutants, suggesting no increase in lipid peroxidation or oxidative stress (compare O,U with P-T). Note that sequential rounds of IF allow the sections to be labeled with Trp53 and pH3 and some sections thus look very similar to those used in Fig. 3F,G. Scale bars: 50 µm.

oxidative stress, which contributes to lipid peroxidation and leads to the generation of 4-hydroxynonenal (4HNE) (Zhong and Yin, 2015). To assess oxidative stress, the presence of 4HNE was examined in mutants and littermate embryos. This analysis revealed no significant differences in 4HNE levels or localization in Mrp null embryos (compare Fig. 4O″,U″ with Fig. 4P″-T″), suggesting that excessive oxidative stress does not contribute to the mutant phenotype.

Next, the mitochondrial morphology in mutant and control embryos was carefully examined using transmission electron microscopy (TEM). As mentioned earlier, changes in mitochondrial morphology depending on the stage of development have been previously documented (Lima et al., 2018). TEM revealed that mitochondria in mutant embryos were dramatically different from those in littermates at E7.5 (Fig. 5A-F). Although controls clearly displayed numerous regularly stacked cristae, each Mrp mutant

Development (2020) 147, dev188714. doi:10.1242/dev.188714

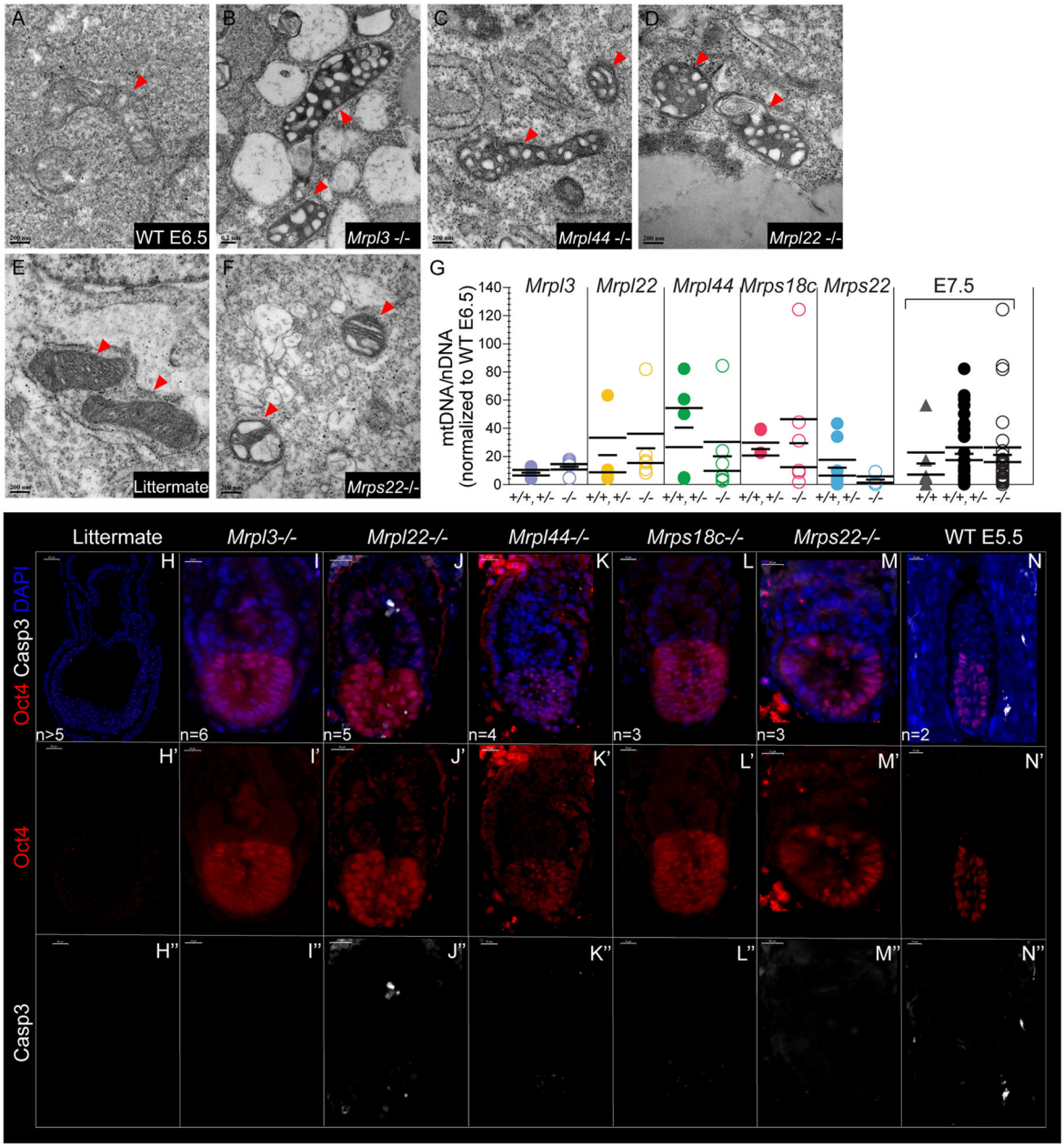

Fig. 5. Mrp null mitochondria are present with abnormal morphology but mutants do not show a dramatic increase in active caspase 3. (A-F) TEM images reveal the drastic difference in mitochondrial morphology between mutants and control embryos (compare A,E with B-D,F). The mitochondria of mutants have far fewer cristae and contain large vesicle-like structures. Red arrowheads point to mitochondria. (G) qPCR from single embryos was performed to determine the ratio of mitochondrial and nuclear genomic DNA. No significant difference is observed in the ratio of mitochondrial to nuclear genome content between mutants and littermates, with $P>0.05$ in all comparisons (*t*-test). Results are shown as mean±s.e.m. Data color code: *Mrpl3*, purple; *Mrpl22*, yellow; *Mrpl44*, green; *Mrps18c*, red; *Mrps22*, blue; wild-type E7.5 embryos, gray triangles; E7.5 littermates, black circles; E7.5 mutants, white circles. Number of individual embryos: *Mrpl3* +/+, +/– $n=4$ and –/– $n=7$; *Mrpl22* +/+, +/– $n=4$ and –/– $n=6$; *Mrpl44* +/+, +/– $n=5$ and –/– $n=7$; *Mrps18c* +/+, +/– $n=3$ and –/– $n=6$; *Mrps22* +/+, +/– $n=8$ and –/– $n=3$; and wild-type E6.5 $n=2$. (H-N) Embryos labeled with anti-active-caspase-3 antibody (white), Oct4 (red) and DAPI (blue). Few cells positive for actived caspase-3 are present in embryos, regardless of genotype (including null mutants). +/+, wild-type embryos; +/–, heterozygous embryos; –/–, mutant embryos. Scale bars: 200 nm in A-F; 50 µm in H-H″; 20 µm in I-N″.

instead had many vesicle-like structures within every mitochondria (arrows in Fig. 5B-D,F), similar those observed in cells undergoing apoptosis (Sun et al., 2007; Yamaguchi and Perkins, 2009).

During apoptotic progression, mitochondria undergo swelling, presumably resulting in the vesicle-like phenotype and eventual bursting of the organelle (Sun et al., 2007). Because abnormal mitochondrial morphology was observed, it was of interest to determine whether the total mitochondrial content was altered in the absence of Mrp genes. Therefore, quantitative PCR (qPCR) was performed to examine the ratio of mitochondrial DNA versus nuclear DNA. qPCR analysis from embryos dissected at E7.5 revealed that there was no significant difference in the mitochondrial to nuclear genome ratio between mutants and littermates (Fig. 5G). This result suggests that, despite severely irregular mitochondrial morphology, mitochondrial biogenesis and the total number of organelles or mitochondrial genomes was not altered in mutant embryos.

Development (2020) 147, dev188714. doi:10.1242/dev.188714

Based on the vesicle-like phenotype displayed in mutant mitochondria, the localization of activated caspase-3 in the mutant embryos was examined. Surprisingly, in spite of the pronounced mitochondrial morphology in the mutants, only a few cells positive for activated caspase-3 were found in the embryonic portion and no activated caspase-3 fluorescent signal was present in the extraembryonic portion of the mutant embryos (compare Fig. 5H″, N″ with Fig. 5I″-M″). Quantification revealed that Mrp knockout mutants contained an average of 3.5 actived caspase-3 positive cells per 100 cells counted whereas littermate and stage-matched controls had 1.7 actived caspase-3 positive cells per 100 cells counted (data not shown). Although this difference was statistically significant (P=0.02), we do not believe this slight increase in caspase-3 mediated apoptosis is a major factor contributing to the overall mutant phenotype.

Because the mutant embryos had altered mitochondrial morphology, the OXPHOS output was assessed by measuring ATP and ADP levels. Healthy proliferating cells contain significantly less ADP than ATP. In apoptotic cells, the ATP level drastically decreases, resulting in an altered ADP to ATP ratio (Crouch et al., 1993). To investigate mitochondrial function, the ratio of ADP to ATP was measured in individual embryos. All homozygous knockout embryos had a significantly higher ADP to ATP ratio compared with littermates (Fig. 6A). Because the changes in ADP to ATP ratio may be attributed to developmental stage, the same assays were also performed on individual wild-type E5.5 embryos as stage-matched controls for Mrp mutants. However, no difference between wild-type E5.5 and E7.5 littermate embryos (either +/+ or +/−) was found. Thus, we conclude that the altered ADP to ATP ratio in mutants is reflective of mitochondrial disfunction rather than a consequence of developmental delay. Together these data indicate that Mrp mutants fail to produce normal levels ATP, which probably limits continued development.

Knowing that mitochondrial morphology and function are impaired in Mrp mutants, and that MRPs are components of mitoribosomes, which are responsible for translation of all genes encoded in the mtDNA, we examined the presence of mtCO2, subunit II of cytochrome c oxidase, a mitochondrial-encoded

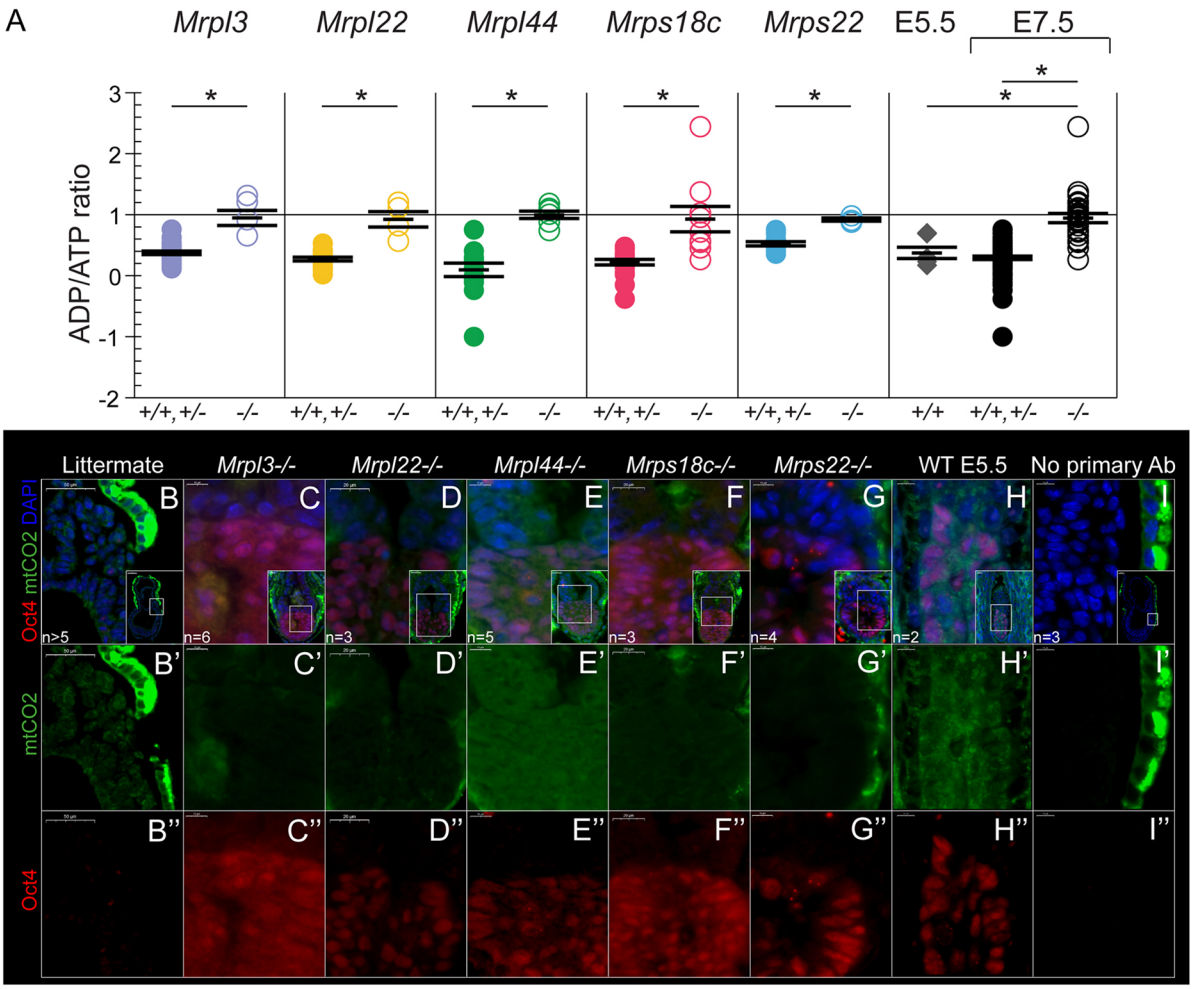

Fig. 6. Mrp mutants have less ATP and defective mitochondrial translation. (A) Mutant embryos have a significantly higher ADP to ATP ratio, indicating reduced levels of ATP in null cells (*P<0.05). This difference remains when comparing with wild-type E5.5 stage-matched embryos. Results are shown as mean±s.e.m. Data color codes as in Fig. 5G. Number of individual embryos: *Mrpl3* +/+, +/– n=24 and –/– n=5; *Mrpl22* +/+, +/– n=18 and –/– n=4; *Mrpl44* +/+, +/– n=13 and –/– n=6; *Mrps18c* +/+, +/– n=20 and –/– n=9; *Mrps22* +/+, +/– n=10 and –/– n=3; wild-type E5.5 n=6. (B-H) Embryos were labeled with anti-mtCO2 (green), Oct4 (red) and DAPI (blue). mtCO2 can be seen throughout littermate and stage-matched controls but is largely absent in null cells (compare B,H with C-G). (I) Control with no primary antibody added. The green signal observed in the visceral endoderm is the result of secondary antibody binding to endogenous mouse immunoglobulin G. +/+, wild-type embryos; +/–, heterozygous embryos; –/–, mutant embryos. Scale bars: 50 µm in B-B″ (inset, 100 µm); 20 µm in D-D″ (inset, 20 µm), F-F″; 10 µm in C-C″ (inset, 20 µm), E-E″ (inset, 20 µm), G-G″ (inset, 20 µm), H-H″ (inset, 20 µm) and I-I″ (inset, 50 µm).

Development (2020) 147, dev188714. doi:10.1242/dev.188714

component of the ETC. As shown in Fig. 6B″-H″, mtCO2 was observed throughout littermate and stage-matched control embryonic cells but was absent in each homozygous mutant, indicating that no mtCO2 protein was present and that mitochondrial translation was defective in the absence of Mrp genes.

Previous *Xenopus* studies reveal that inhibition of mitochondrial ROS production results in cell cycle arrest by preventing the activation of Cdc25c, a phosphatase that triggers entry into mitosis, a crucial role in the G2/M checkpoint (Han et al., 2018; Peng et al., 1997, 1998). Because Mrp mutants have a defective ETC, which limits the production of ROS, we examined the phosphorylation status of Cdc25c in the mutant embryos. Prior to the G2/M checkpoint, Cdc25c is kept inactive by phosphorylation on its inhibitory site, serine 216 (S216), which promotes binding to a 14-3-3 protein (Peng et al., 1998, 1997; Kumagai et al., 1998). Upon mitosis, the inhibitory site of Cdc25c is dephosphorylated by protein phosphatase 2A and hyperphosphorylated by kinases such as Cdc2/cyclin B at the serine/threonine residues (Hoffmann et al., 1993; Kumagai et al., 1998; Clarke et al., 1993; Izumi and Maller, 1993; Strausfeld et al., 1994; Roshak et al., 2000). Examination of phosphorylated S216 [phospho-Cdc25c (S216)] revealed significantly more foci in Mrp mutants than in littermate and stage-matched controls (Fig. 7A-E). These results indicate that abrogation of each Mrp gene not only alters energy production, but also leads to cell cycle arrest at the G2/M checkpoint. This cell cycle disruption is probably a major contributing factor to the overall arrested development and failure to initiate gastrulation.

DISCUSSION

MRPs play evolutionarily conserved essential roles. Along with ribosomal RNAs, the MRPs constitute the mitoribosome complex leading to the coordinated synthesis of ETC proteins, primary components of the OXPHOS system. Because of the important role in cellular energy production, defects in the ETC are often associated with mitochondrial diseases (De Silva et al., 2015). The connection between Mrp mutation and human diseases has been well documented in multiple clinical studies. Many studies utilize plant and *Drosophila* model systems to explore the involvement of Mrp genes in development, but studies identifying the roles of Mrp genes in mammalian embryogenesis are conspicuously absent (Frei et al., 2005; Robles and Quesada, 2017). Presented here is *in vivo* analysis of mouse embryos that lack both alleles of individual Mrp genes. The data demonstrate the indispensable role of individual Mrp genes during early mammalian development and that loss of each Mrp leads to severe developmental delay and a failure to initiate gastrulation. Together these data suggest that, despite the presence of 70 Mrp genes, each has a distinct role with little or no functional redundancy among the Mrp group.

These early lethal phenotypes correlate well with previous knockout mouse studies that show the importance of multiple mitochondria-associated genes during embryogenesis (Piruat et al., 2004; Baker and Ebert, 2013; Li et al., 2000; Chen et al., 2003; Wakabayashi et al., 2009; Davies et al., 2007; Hance et al., 2005; Humble et al., 2013; Nonn et al., 2003; Conrad et al., 2004; Larsson et al., 1998; Yagi et al., 2012; Park et al., 2007; Cerritelli et al., 2003; Steenbergen et al., 2005; Kim et al., 2007). Specifically, in the absence of *Sdh*, a gene that encodes for a subunit within complex II of the ETC, embryos cannot be found at E9.5, indicating earlier lethality (Piruat et al., 2004). Additionally, similar to the Mrp homozygous knockout embryos we examined in depth herein, embryos lacking both alleles of other nuclear-encoded mitochondrial functioning proteins, including *Nars2*, *Ndufa9*, *Ndufs8*, and *Timm22*, were also found to display comparable E7.5 phenotypes; that is, formation of an egg cylinder but lack of gastrulation features (Fig. 8; blogs.umass.edu/jmager). These data further illustrate the importance of a functioning OXPHOS system during the peri-gastrulation.

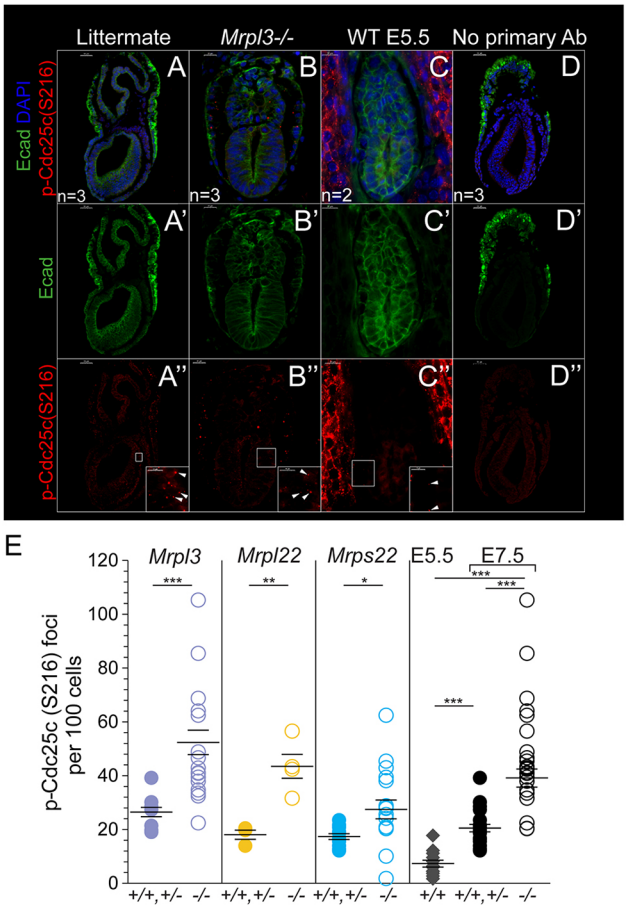

Fig. 7. Mrp null cells are stalled at the G2/M transition. (A-C) Sectioned embryos were labeled with E-cadherin (green), phospho-Cdc25c (S216) (red) and DAPI (blue). White arrows point to phospho-Cdc25c (S216) foci. (D) Control with no primary antibody added. Green signal observed in the visceral endoderm is the result of secondary antibody binding to endogenous mouse immunoglobulin G. (E) Quantification reveals that significantly more phospho-Cdc25c foci are present in Mrp null embryos than in littermates or stage-matched controls. Results are shown as mean±s.e.m. ***P<0.0005, **P<0.01, *P<0.05. Color code: *Mrpl3*, purple; *Mrpl22*, yellow, *Mrps22*, blue, wild-type E5.5 embryos, gray diamonds; E7.5 littermate, black circles; E7.5 mutants, white circles. Number of individual embryos: *Mrpl22* +/+, +/– and –/– n=1; *Mrps22* +/+, +/– n=3 and –/– n=4. +/+, wild-type embryos; +/–, heterozygous embryos; –/–, mutant embryos. Scale bars: 50 µm in A-A″ (inset, 10 µm) and D-D″; 20 µm in B-B″ (inset, 10 µm) and C-C″ (inset, 10 µm).

Given the consistency of the ∼E7.5 delay in each of the Mrp knockouts, it is reasonable to hypothesize that Mrp genes are not essential until gastrulation. However, an important caveat is that abundant maternal RNA and proteins are present in oocytes. Thus, maternal MRP protein might promote survival of the Mrp mutant embryos through implantation, resulting in the observed phenotype only after maternal stores have diminished through normal protein turnover. In the absence of individual MRP function, it is possible that maternal MRP provides adequate mitochondrial function and energy production to allow mutant embryos to progress through implantation (approximately 4 days). In this scenario, perhaps the

Development (2020) 147, dev188714. doi:10.1242/dev.188714

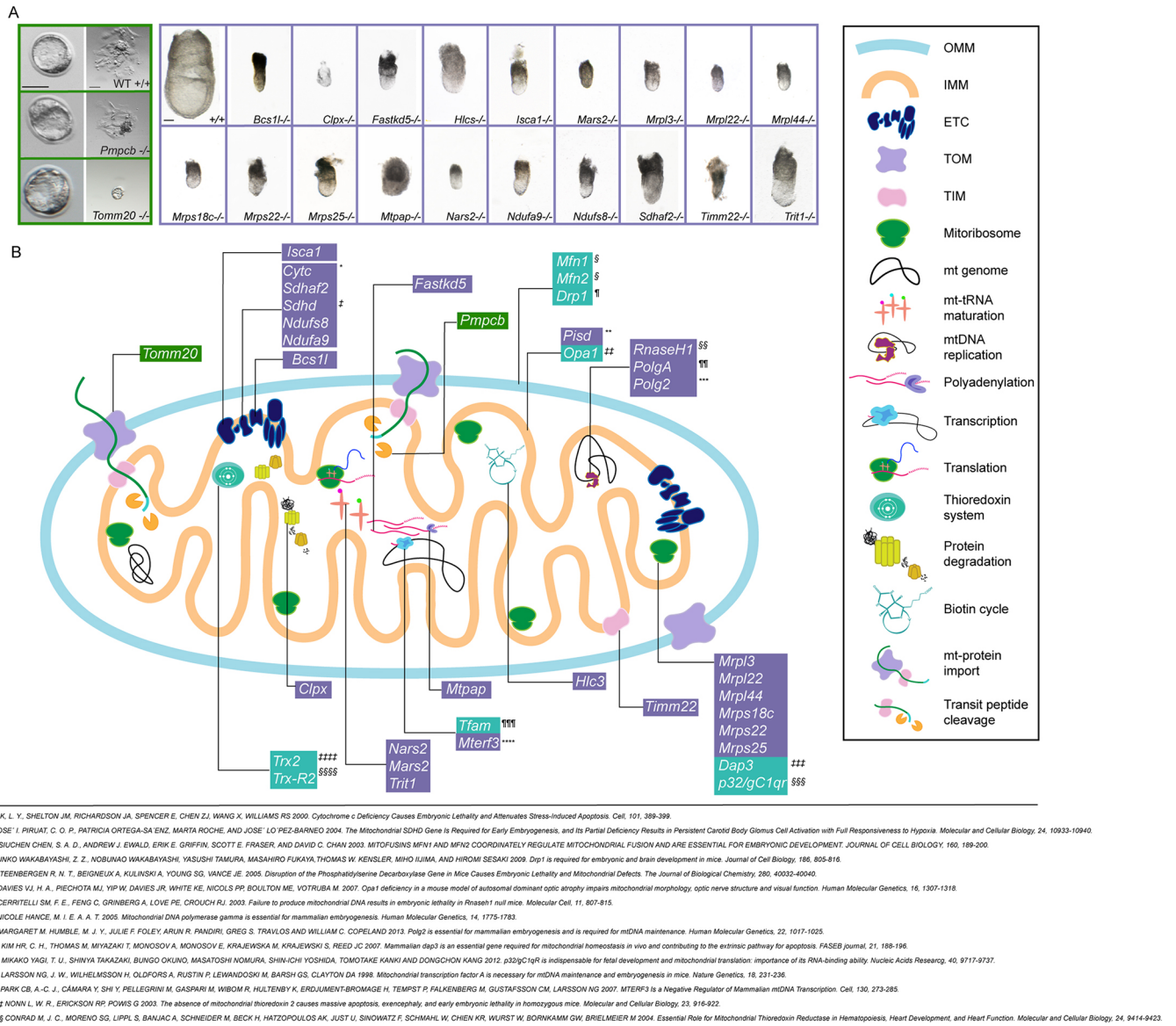

* LI K, L. Y., SHELTON JM, RICHARDSON JA, SPENCER E, CHEN ZJ, WANG X, WILLIAMS RS 2000. Cytochrome c Deficiency Causes Embryonic Lethality and Attenuates Stress-Induced Apoptosis. Cell, 101, 389-399.

‡ JOSE' I. PIRUAT, J. O. P., PATRICIA ORTEGA-SA'ENZ, MARTA ROCHE, AND JOSE' LO'PEZ-BARNEO 2004. The Mitochondrial SDHD Gene Is Required for Early Embryogenesis, and Its Partial Deficiency Results in Persistent Carotid Body Glomus Cell Activation with Full Responsiveness to Hypoxia. Molecular and Cellular Biology, 24, 10933-10940.

§ HSIUCHEN CHEN, S. A. D., ANDREW J. EWALD, ERIK E. GRIFFIN, SCOTT E. FRASER, AND DAVID C. CHAN 2003. MITOFUSINS MFN1 AND MFN2 COORDINATELY REGULATE MITOCHONDRIAL FUSION AND ARE ESSENTIAL FOR EMBRYONIC DEVELOPMENT. JOURNAL OF CELL BIOLOGY, 160, 189-200.

¶ JUNKO WAKABAYASHI, Z. Z., NOBUNAO WAKABAYASHI, YASUSHI TAMURA, MASAHIRO FUKAYA, THOMAS W. KENSLER, MIHO IIJIMA, AND HIROMI SESAKI 2009. Drp1 is required for embryonic and brain development in mice. Journal of Cell Biology, 186, 805-816.

** STEENBERGEN R, N. T., BEIGNEUX A, KULINSKI A, YOUNG SG, VANCE JE. 2005. Disruption of the Phosphatidylserine Decarboxylase Gene in Mice Causes Embryonic Lethality and Mitochondrial Defects. The Journal of Biological Chemistry, 280, 40032-40040.

‡‡ DAVIES VJ, H. A., PIECHOTA MJ, YIP W, DAVIES JR, WHITE KE, NICOLS PP, BOULTON ME, VOTRUBA M. 2007. Opa1 deficiency in a mouse model of autosomal dominant optic atrophy impairs mitochondrial morphology, optic nerve structure and visual function. Human Molecular Genetics, 16, 1307-1318.

§§ CERRITELLI SM, F. E., FENG C, GRINBERG A, LOVE PE, CROUCH RJ. 2003. Failure to produce mitochondrial DNA results in embryonic lethality in Rnaseh1 null mice. Molecular Cell, 11, 807-815.

¶¶ NICOLE HANCE, M. I. E. A. A. T. 2005. Mitochondrial DNA polymerase gamma is essential for mammalian embryogenesis. Human Molecular Genetics, 14, 1775-1783.

*** MARGARET M. HUMBLE, M. J. Y., JULIE F. FOLEY, ARUN R. PANDIRI, GREG S. TRAVLOS AND WILLIAM C. COPELAND 2013. Polg2 is essential for mammalian embryogenesis and is required for mtDNA maintenance. Human Molecular Genetics, 22, 1017-1025.

‡‡‡ KIM HR, C. H., THOMAS M, MIYAZAKI T, MONOSOV A, MONOSOV E, KRAJEWSKA M, KRAJEWSKI S, REED JC 2007. Mammalian dap3 is an essential gene required for mitochondrial homeostasis in vivo and contributing to the extrinsic pathway for apoptosis. FASEB journal, 21, 188-196.

§§§ MIKAKO YAGI, T. U., SHINYA TAKAZAKI, BUNGO OKUNO, MASATOSHI NOMURA, SHIN-ICHI YOSHIDA, TOMOTAKE KANKI AND DONGCHON KANG 2012. p32/gC1qR is indispensable for fetal development and mitochondrial translation: importance of its RNA-binding ability. Nucleic Acids Researcg, 40, 9717-9737.

¶¶¶ LARSSON NG, J. W., WILHELMSSON H, OLDFORS A, RUSTIN P, LEWANDOSKI M, BARSH GS, CLAYTON DA 1998. Mitochondrial transcription factor A is necessary for mtDNA maintenance and embryogenesis in mice. Nature Genetics, 18, 231-236.

**** PARK CB, A.-C. J., CÂMARA Y, SHI Y, PELLEGRINI M, GASPARI M, WIBOM R, HULTENBY K, ERDJUMENT-BROMAGE H, TEMPST P, FALKENBERG M, GUSTAFSSON CM, LARSSON NG 2007. MTERF3 Is a Negative Regulator of Mammalian mtDNA Transcription. Cell, 130, 273-285.

‡‡‡‡ NONN L, W. R., ERICKSON RP, POWIS G 2003. The absence of mitochondrial thioredoxin 2 causes massive apoptosis, exencephaly, and early embryonic lethality in homozygous mice. Molecular and Cellular Biology, 23, 916-922.

§§§§ CONRAD M, J. C., MORENO SG, LIPPL S, BANJAC A, SCHNEIDER M, BECK H, HATZOPOULOS AK, JUST U, SINOWATZ F, SCHMAHL W, CHIEN KR, WURST W, BORNKAMM GW, BRIELMEIER M 2004. Essential Role for Mitochondrial Thioredoxin Reductase in Hematopoiesis, Heart Development, and Heart Function. Molecular and Cellular Biology, 24, 9414-9423.

Fig. 8. Summary of early lethal phenotypes of nuclear-encoded mitochondrial genes. (A) Additional novel phenotypes of null embryos analyzed by our group: E3.5 (green box) and E7.5 (purple box). (B) Mitochondrial localization and function of each protein encoded by nuclear-encoded mitochondrial genes, indicated by black lines. Developmental time points of null embryo lethality are indicated by color: green, developmental arrest at implantation; purple, developmental arrest at E6.5-E8.5; turquoise, ≥E9.5 lethality. Published knockout studies are indicated with the corresponding reference number. The 21 genes without an associated reference are novel phenotypes presented herein. OMM, outer mitochondrial membrane; IMM, inner mitochondrial membrane; ETC, electron transport chain; TOM, translocase of the outer membrane; TIM, translocase of the inner membrane. Scale bars: 50 µm (E3.5 blastocyst) and 100 µm (outgrowth colony) in green box; 100 µm (E7.5 embryos) in purple box.

mitochondrial function of Mrp mutants wanes significantly at E5.5 as maternal mRNA and protein is exhausted, slowing or stopping cell division and morphogenetic movements and resulting in the egg-cylinder arrest observed. Because Mrp null embryos develop normally for ∼6 days, it is unlikely that the maternal protein persists for that long and that Mrp gene function is not required for egg cylinder formation. However, without formal demonstration of protein half-life and maternal deletion experiments, there remains the question of precisely when during development MRP proteins are required.

The metabolic analysis performed here reveals that the ADP to ATP ratio is significantly increased in all of the Mrp mutants. In healthy proliferating cells, the ATP concentration is much higher than that of ADP, resulting in an ADP/ATP ratio close to 0.5 in control embryos. All of the Mrp mutant embryos examined had similar ADP/ATP ratios of close to 1.0. These results suggest that ATP production is deficient in the absence of functional MRP proteins. The OXPHOS system requires the translation of essential ETC components within mitochondria. Our data show that lack of functional MRP proteins leads to disruption of the mitochondrial translation machinery and therefore a lack of ETC related proteins, as reflected by the absence of mtCO2 protein in mutant cells (Fig. 6C′-G′). The absence of functional ETC components, in turn, is most likely responsible for the drastic reduction of ATP in mutant embryos. The aberrant mitochondrial morphology observed in each of the Mrp mutants provides further support for defects in

Development (2020) 147, dev188714. doi:10.1242/dev.188714

mitochondrial function. Given these defects, it is somewhat surprising that the number of mitochondria (inferred from the mtDNA/gDNA ratio; Fig. 6) in mutant cells was unaltered at E7.5, indicating that biogenesis of mitochondria in mutants is unaffected and that the defective mitochondria are not being degraded.

The excessive amount of vesicle-like structures in the mitochondria of individual mutants is a phenotypic phenomenon associated with apoptosis, which also results in cytochrome c release and activation of caspase-3. Becase no elevation in the number of actived Trp53-positive cells was observed in mutants, the presence of activated caspase-3 was investigated given the aberrant mitochondrial morphology of the mutants. Surprisingly, very few cells positive for actived caspase-3 were present in any of the Mrp mutants, suggesting that apoptosis is not a major factor in the mutant phenotypes. At E7.5, the mutant cells appear to be proliferating as a large number of pH3-positive cells were detected in the embryos; however, at late E8.5 and E9.5, the mutants are completely reabsorbed. The results show that development of the mutant embryos occurs normally until ∼E6.0 when developmental progression stalls at the early-egg cylinder stage; cell death and resorption do not finally occur until ∼E8. Because ATP is required for the activation of caspase-3, the lack of activated caspase-3 positive cells in the Mrp mutants might be the result of insufficient cytosolic ATP (Liu et al., 1996; Li et al., 1997). If this is the case, addition of exogenous ATP may be sufficient to restore the caspase-3 mediated apoptotic pathway.

Aside from affecting the energy content, disruption of the OXPHOS system can also impact cellular signaling. A byproduct of the respiratory chain is ROS. Although excessive ROS leads to oxidative stress, it is also an essential second messenger associated with cell cycle progression and several signaling pathways such as NF-kB and MAPK pathways (Zhang et al., 2016; Boonstra and Post, 2004). Lipid peroxidation as a result of elevated ROS level is not observed in the mutants. This result is not unexpected as ROS is a byproduct during the transfer of electrons in the ETC, and we have shown that crucial ETC components are not translated in mutant embryos, most likely resulting in a failure of ETC altogether.

In vivo studies utilizing *Xenopus* embryos have shown that inhibiting mitochondrial ROS production in the ETC can also lead to cell cycle arrest by disrupting the activation of Cdc25c, a phosphatase that triggers the entry of mitosis (Han et al., 2018). Many studies have shown that embryos increase in size significantly during gastrulation as a result of rapid cell cycles (Mac Auley et al., 1993; Snow, 1977; Power and Tam, 1993). Here, we show that Cdc25c phosphorylated at serine 216 [phospho-Cdc25c (S216)] foci are significantly elevated throughout Mrp mutant embryos, suggesting cell cycle arrest. Furthermore, although there are pH3-positive cells in the mutants, the majority of pH3 signal cells appear to have a less condensed chromatin structure than littermates, similar to the structure observed in the late G2 phase of the cell cycle. However, a more detailed assessment of the cell cycle stage is necessary to conclude precisely when Mrp mutant cells may be arrested. Together, these data suggest that when mitochondrial translation is obstructed, the overall energy content in the embryos decreases, which in turn limits the generation of ROS. As a result, regulation of Cdc25c is altered, perturbing cell cycle progression and resulting in the Mrp mutant phenotype, exhibiting a failure to grow and initiate gastrulation.

Mitochondria are tightly regulated organelles that can swiftly achieve conformational and functional adjustments in response to changes in the cellular environment and signaling (Fu et al., 2019; Jornayvaz and Shulman, 2010; Yao et al., 2019). As the primary source of ATP and a hub for many biosynthetic and metabolic pathways, viability is dependent on intact and functional mitochondria (Fu et al., 2019; Chandel, 2015; Tait and Green, 2012; De Silva et al., 2015; Lee and Han, 2017). Some previous knockout studies have highlighted the importance of mitochondrial function for successful embryo development (Barak et al., 1999; Chen et al., 2003; Wakabayashi et al., 2009; Humble et al., 2013; Li et al., 2000; Piruat et al., 2004; Steenbergen et al., 2005; Davies et al., 2007; Cerritelli et al., 2003; Hance et al., 2005; Park et al., 2007; Kim et al., 2007; Yagi et al., 2012; Nonn et al., 2003; Conrad et al., 2004; Larsson et al., 1998). These studies, combined with the analysis presented here of 21 novel knockout alleles in mitochondrial genes (5 presented in depth, 16 in Fig. 8 and in blogs.umass.edu/jmager), indicate that disrupting components of the ETC, mitochondrial translation machinery or other components of mitochondria most often results in arrest immediately prior to gastrulation (Fig. 8). This is perhaps not surprising as mitochondria are essential for both cell movement and rapid proliferation, and gastrulation is the time of dynamic morphogenetic movements and extensive embryo growth (Ratnaparkhi, 2013; Yao et al., 2019; Fu et al., 2019). As presented above, the knockout of single Mrp genes was found to interfere with mitochondrial translation, a decrease in energy production and cell cycle perturbation, combining to result in growth arrest and a failure to initiate gastrulation.

One in 4300 people are affected by mitochondrial diseases, the most common type of genetic disorder (Schaefer et al., 2019; Ng and Turnbull, 2016). Of the 37 genes mentioned in Fig. 8, 36 are associated with human diseases, the majority of which are monogenic such as combined oxidative phosphorylation deficiency (COXPD), multiple mitochondrial dysfunctions syndrome (MMDS) and a variety of neural and cardio-related disorders (Dickinson et al., 2016; 2020). These mouse models provide insight into the pathological mechanisms of these mitochondrial diseases during embryonic and neonatal development.

Although it is well documented by others that mammalian embryos utilize glycolysis as the primary energy source during development, the study here highlights the indispensable role of a functional OXPHOS system for the initiation of gastrulation. This study also supports the idea that distinct energy systems are required at different time points during development. The survival of mutant embryos through implantation and egg cylinder formation indicates either that maternal Mrp genes contribute and/or that an alternative energy system such as glycolysis drives developmental progression prior to gastrulation. To better understand the regulation and requirements of each cellular energy system it would be of interest to study the ATP source during a variety of embryonic stages, as well as temporal and tissue-specific conditional knockout strategies.

MATERIALS AND METHODS

Animals

Use of animals was approved by the University of Massachusetts Institutional Use and Care of Animals Committee (IUCAC). The Mrp knockout alleles were generated by the Jackson Laboratory (stock no. 048652-UCD KOMP: C57BL/6N-*Mrpl3*$^{em1(IMPC)J}$/Mmucd; 048651-UCD KOMP: C57BL/6N-A^{tm1Brd} *Mrpl22*$^{tm1b(KOMP)Mbp}$/JMmucd; 048654-UCD KOMP: C57BL/6N-*Mrpl44*$^{em1(IMPC)J}$/Mmucd; 048660-UCD KOMP: C57BL/6N-*Mrps18c*$^{tm1.1(KOMP)Vlcg}$/JMmucd; and 048661-UCD KOMP: C57BL/6N-*Mrps22*$^{tm1.1(KOMP)Vlcg}$/JMmucd). In brief, the *Mrpl3* and *Mrpl44* knockout alleles were generated by removing exon 2 (185 bp and 1424 bp, respectively) in the genomic sequences using CRISPR/Cas system; whereas *Mrpl22*, *Mrps18c* and *Mrps22* knockout alleles were generated by removing exon 3, exons 1-6 and exons 1-8, respectively, and

Development (2020) 147, dev188714. doi:10.1242/dev.188714

replacing part of the genomic locus with the *lacZ* reporter in C57BL/6NJ mouse embryonic stem cells (Fig. 1).

The knockout alleles used to generate null embryos shown in Fig. 8 were generated by the Jackson Laboratory (JAX) or University of California, Davis, CA, USA (UCD): C57BL/6N- *Bcs1l*$^{tm1.1(KOMP)Vlcg}$; 047134-UCD KOMP: C57BL/6N-*Clpx*$^{tm1.1(KOMP)Vlcg}$/JMmucd; 047662-UCD KOMP: C57BL/6N-*Fastkd5*$^{tm1.1(KOMP)Vlcg}$/JMmucd; 42127-JAX: C57BL/6NJ-*Hlcs*$^{em1(IMPC)J}$/Mmjax; MMRRC: 048244-UCD KOMP: C57BL/6N-A^{tm1Brd} *Isca1*$^{tm1b(KOMP)Wtsi}$/JMmucd; 048536-UCD KOMP: C57BL/6N-*Mars2*$^{tm1.1(KOMP)Vlcg}$/JMmucd; C57BL/6N-*Mrps25*$^{tm1.1(KOMP)Vlcg}$/JMmucd; Produced by UCD: C57BL/6N- *Mtpap*$^{tm1.1(KOMP)Vlcg/MbpCrl}$; 048737-UCD KOMP: C57BL/6N-*Nars2*$^{em1(IMPC)J}$/Mmucd; 42355-JAX: C57BL/6NJ-*Ndufa9*$^{em1(IMPC)J}$/Mmjax; 048764-UCD KOMP: C57BL/6N-*Ndufs8*$^{em1(IMPC)J}$/Mmucd; 42307-JAX: C57BL/6NJ-*Sdhaf2*$^{em1(IMPC)J}$/Mmjax; 050059-UCD KOMP: C57BL/6N-*Timm22*$^{tm1b(KOMP)Wtsi}$/JMmucd; 050225-UCD KOMP: C57BL/6N-*Trit1*$^{tm1.1(KOMP)Vlcg}$/JMmucd; Produced by Baylor College of Medicine, TX, USA (BCM): C57BL/6N-*Pmpcb*$^{tm1b(EUCOMM)Hmgu}$; and 43742-JAX: C57BL/6NJ-*Tomm20*$^{em1(IMPC)J}$/Mmjax. All results shown were repeated on a minimum of three mutant and control embryos from each knockout line, except for the *Mrpl22* knockout line shown in Fig. 7E. Further data on each of the phenotypes of the homozygous embryos from each of these strains is available at blogs.umass.edu/jmager.

Embryo retrieval and genotyping

Mrp null embryos were generated by heterozygote intercrosses. Heterozygous males and females were housed together, and the morning of the copulation plugs was defined as E0.5. Genotypes of individual embryos were determined by PCR using the following primers: *Mrpl3*, wild-type (5′-CTGTCAAGTACAGATTCATGTGG-3′ and 5′-TGGTTCCCAGGGATGTAAAG-3′) and knockout (5′-CTGTCAAGTACAGATTCATGTGG-3′ and 5′-TCTGGAACTATGCTTCCCAAAC-3′); *Mrpl22*, wild-type (5′-AAAACCCATTTCAGTCCTGAGT-3′ and 5′-TCACAGCAGGGTGACAGAAC-3′) and knockout (5′-CGGTCGCTACCATTACCAGT-3′ and 5′-GCAGCCTGGTCCATAGAGTG-3′); *Mrpl44*, wild-type (5′-ACGGACTGCCAGTGGTTATC-3′ and 5′-AACTAGACTCTCAGTGCCTTCG-3′) and knockout (5′-ACGGACTGCCAGTGGTTATC-3′ and 5′-AACCTCCAGCACTCACAACC-3′); *Mrps18c*, wild-type (5′-CACATTGATTGCTTGTTATTTCG-3′ and 5′-CAGTTGAGTGCAGATGCTTG-3′) and knockout (5′-CGGTCGCTACCATTACCAGT-3′ and 5′-CGGTGTCCAGAGAACACTCA-3′); and *Mrps22*, wild-type (5′-GCTGTGGGCAGTGTTATTGT-3′ and 5′-TCTCACACCTAGTACCGCAGTC-3′) and knockout (5′-CGGTCGCTACCATTACCAGT-3′ and 5′-TCAGTAAGTACCTTTTAATCCCAAGA-3′). Specific genotyping protocol is available at https://www.mmrrc.org/. All results shown were repeated on a minimum of three mutant embryos.

Additional homozygous knockout mouse embryos displayed in Fig. 8 were generated by heterozygote intercrosses as above. Genotypes of individual embryos were determined by PCR. Specific genotyping protocol is available at https://www.mmrrc.org/.

All results presented were repeated on a minimum of three mutants and three controls from each knockout line, except for *Mrpl22* knockout mutants shown in Fig. 7E or unless specified. All assays were also assessed for differences between wild-type and heterozygous embryos but no significant differences were observed.

RNA extraction and RT-PCR analysis

Total RNA was isolated from mouse tissues using Roche High Pure RNA Isolation Kit (Roche 11828665001) and was converted to cDNA using BioRad iScript cDNA Synthesis (BioRad 1708890). RT-PCR was performed for 35 cycles of 30 s at 60°C, 72°C and 95°C with the following primers (5′ to 3′) unless otherwise specified: *Mrpl3* (292 bp), 5′-TTGGTGGGATGAACATCTTTC-3′ and 5′-GGCTGCGATTTTTCCATTAT-3′; *Mrpl22* (542 bp), 5′-GGGTGCACTGAGGGTACCTA-3′ and 5′-CGTGGTCAACTGCTGTCTTG-3′; *Mrpl44* (620 bp), 5′-GGGGAGTGAAGAAGGGATTC-3′ and 5′-TACGACGGTCCACATCTCAA-3′; *Mrps18c* (354 bp), 5′-GGTTGCTCTGTGCAGTGGTA-3′ and 5′-TGGCATAAACCCCATTTTCT-3′; *Mrps22* (533 bp), 5′-TACAACCACTGAAGCCACCA-3′ and 5′-AGCCATTCCACCAAAGTGTC-3′; *brachyury* (*T*) (313 bp), 5′-CATGTACTCTTTCTTGCTGG-3′ and 5′-GGTCTCGGGAAAGCAGTGGC-3′; *Gapdh* (452 bp), 5′-ACCACAGTCCATGCCATCAC-3′ and 5′-TCCACCACCCTGTTGCTGTA-3′.

Whole mount *in situ* hybridization

Embryos were freshly dissected and fixed in 4% paraformaldehyde for 2-4 h on ice as described by Tremblay et al. (2001). Embryos were then dehydrated in a methanol series and stored for up to 1 month. Embryos were rehydrated in a methanol series in 1× phosphate-buffered saline with Tween 20 (PBT), rinsed twice in 1× PBT for 5 min and bleached in 6% hydrogen peroxide for 1 h. Embryos were then rinsed with 1× PBT, treated with proteinase K for 6-8 min and incubated with glycine in 1× PBT for 5 min. After rinsing twice with 1× PBT for 5 min, embryos were fixed with 4% paraformaldehyde with 0.02% glutaraldehyde for 20 min. Embryos were rinsed twice in 1× PBT for 5 min and incubated in 1:1 hybridization buffer (50% formamide, 5× SSC, 0.1% Tween 20, 0.1% SDS, 50 µg/ml heparin, 50 µg/ml yeast tRNA and 60 mM citric acid)/PBT for 10 min, and subsequently in hybridization buffer for 10 min. The embryos were then incubated with 150 ng RNA probes in hybridization buffer at 70°C overnight. The next day, embryos were washed with solutions containing formamide, 20× saline-sodium citrate, 1 M citric acid, 20% SDS and Tween-20 for 30 min at 70°C for the first three washes and at 65°C for the last three washes. Following this, the embryos were rinsed three times in 1× maleic acid buffer containing levamisole for 5 min. The embryos were then blocked in maleic acid buffer with 2% Boehringer blocking reagent for 1 h at room temperature, and then incubated with the antibody solution containing Anti-Digoxigenin-AP (Roche, 11093274910, 1:2000), heat inactivated sheep serum (Sigma-Aldrich, S2263, 1:400) and levamisole (Sigma-Aldrich, L9756, 1%) at 4°C overnight. The following day, the embryos were washed six times with 1× maleic acid buffer containing levamisole for at least 1 h. The embryos were then rinsed three times with alkaline phosphatase buffer containing 1 M Tris-HCl (pH 9.5), 5 M NaCl, 1 M $MgCl_2$ and Tween 20 for 10 min and developed in BM purple solution (Roche, 11442074001) until the color has developed. The embryos were then washed with 1× PBT containing 0.5 M EDTA, fixed in 4% paraformaldehyde overnight, dehydrated in an ethanol series, cleared in xylene, embedded with paraffin and sectioned at 7 µm thick. Antisense probes were generated using E7.5 embryonic cDNA. RT-PCR was performed for 35 cycles of 30 s at 60°C, 72°C and 95°C with the following primers with indicted genes. The amplicons were then cloned into the TOPO-TA Cloning Vectors using the TOPO TA Cloning kit for Sequencing (Invitrogen, 450030) according to the manufacturer's instructions. Plasmid DNA was extracted using QIAprep Spin Miniprep Kit (Qiagen, 27106) and confirmed by sequencing. Plasmids were then linearized with *Pst*I-HF restriction enzyme. Transcription *in vitro* was carried out using DIG RNA Labeling Kit (SP6/T7) (Roche, 11175025910) and the RNA probe confirmed using gel electrophoresis. The probe used was *Mrps22* (intron spanning primers designed to generate an amplicon that includes exon2 to exon6; 533 bp).

X-gal staining

Embryos were freshly dissected and fixed in X-gal (5-bromo-4-chloro-3-indolyl-β-D-galactopyranoside) buffer (PBS with 5 mM EGTA, 2 mM $MgCl{\cdot}6H_2O$, 0.2% NP-40, 0.2 mM deoxycholate) containing 0.2% glutaraldehyde and 1% formaldehyde on ice for 15 min and subjected to modification from Tremblay et al. (2001). In brief, the fixed embryos were washed three times with X-gal buffer for 10 min and stained with X-gal stain (X-gal buffer, 5 mM potassium ferricyanide, 5 mM potassium ferrocyanide, 0.5 mg/ml X-gal) overnight at 37°C. Subsequently, embryos were dehydrated in ethanol, cleared in xylene, embedded with paraffin, and sectioned at 7 µm thick. Sections were deparaffinated and rehydrated for subsequent processing. Eosin staining was performed by immersing rehydrated sectioned embryos in eosin Y solution for 15-20 s, followed by 95% ethanol for 2 min, then 100% ethanol for 2 min and lastly cleared in xylene. Slides were then sealed with Cytoseal 60 (Fisher Scientific 18006) and imaged with a Panoramic MIDI II slide scanner (3dHistech).

Immunofluorescence

Freshly dissected embryos were fixed in 4% paraformaldehyde overnight, dehydrated in ethanol, cleared in xylene, embedded with paraffin and

Development (2020) 147, dev188714. doi:10.1242/dev.188714

sectioned at 7 µm. The sections were deparaffinated in xylene and rehydrated for subsequent procedures. Antigen retrieval was performed by boiling in 0.01 M Tris-Base (pH 10) with 0.05% Tween 20 for 4 min and then allowed to cool to room temperature. The slides were then rinsed twice with 1× PBT for 2 min and blocked in 1× PBT containing 5% non-fat milk for 2 h at room temperature. Primary antibodies were then diluted with 1× PBT containing 5% non-fat milk and added onto the slides. The slides were subsequently incubated at 4°C overnight in a humid chamber, rinsed three times with 1× PBT for 15 min, and then incubated with secondary antibodies at room temperature for 1 h in a humid chamber. Subsequently, the slides were rinsed three times with 1× PBS for 15 min. Nuclei were counterstained with DAPI in PBS (1:10,000) for 3 min. Slides were rinsed with 1× PBS and sealed with ProLong Gold. Immunofluorescence slides were imaged with a Panoramic MIDI II slide scanner (3dHistech).

Sequential rounds of IF were performed to allow the same embryo sections to be labeled with Oct4 and T or with Trp53, pH3 and 4HNE. Once the IF slides were imaged, they were soaked in 1× PBT until the glass coverslips detached from the slides. The slides were soaked in water for 3 min before beginning the second round of IF starting at antigen retrieval step (as listed above).

Primary antibodies against the following were used: T (1:100; Santa Cruz, sc-17743), E-cadherin (1:1000; BD Bioscience,s 610181), Oct4 (1:500; Abcam, ab27985), 4-hydroxynonenal (1:150; Abcam, ab46545), Trp53 (1:100; Cell Signaling Technology, 9284S), pH3 (1:500; Abcam, ab5176), mtCO2 (1:200; Abcam, ab110266), cleaved caspase-3 (1:500; Cell Signaling Technology, 9664S) and phospho-Cdc25c (S216) (1:50; Biorbyt, orb159479). Secondary antibodies used were Alexa Fluor 488 donkey anti-mouse (1:500; Thermo Fisher Scientific, A-21202), Alexa Fluor 647 donkey anti-goat (1:500; Thermo Fisher Scientific, A-21447) and Alexa Fluor 546 donkey anti-rabbit (1:500; Thermo Fisher Scientific, A10040). DAPI (Molecular Probes) concentration was 1:10,000.

Transmission electron microscopy

Freshly dissected mouse embryos were immersed in 2.5% glutaraldehyde in 0.1 M sodium cacodylate buffer (pH 7.2) and fixed overnight at 4°C. Samples were processed and analyzed at the University of Massachusetts Medical School Core Electron Microscopy Facility according to standard procedures. Briefly, the samples were rinsed four times in the same fixation buffer and post-fixed with 1% osmium tetroxide for 1 h at room temperature. Samples were then washed three times with DH_2O for 10 min and then dehydrated through a graded ethanol series of 10% through 95% at 20% increments, before three changes in 100% ethanol. The samples were then infiltrated with two changes of 100% propylene oxide and then with a 50/50% propylene oxide/SPI-Pon 812 resin mixture. The following day, four changes of fresh 100% SPI-Pon 812 resin were made before the samples were polymerized at 70°C in flat embedding molds. The samples were then reoriented and thick sectioned to the correct depth, at which point thin sections of approximately 70 nm were collected and placed on copper support grids and contrasted with lead citrate and uranyl acetate. Sections were examined using the Phillips CM10 with 80 Kv accelerating voltage; images were captured using a Gatan TEM CCD camera.

Real-time qPCR analysis

Dissected embryos were incubated in lysis buffer [50 mM Tris HCl (pH 8.8), 1 mM EDTA (pH 8.0), 0.5% Tween20] with the addition of proteinase K solution (Promega, MC5008) at 55°C for 1 h or overnight and subsequently incubated at 95°C for 10 min. Embryo lysates were then used as template for qPCR. To determine the ratio between mitochondrial genome and nuclear genome using primers to amplify 415 bp of mt-genomic-*CO2* (5′-TTGGTCTACAAGACGCCACA-3′ and 5′-GGTAGCTGTTGGTGGGCTAA-3′) and 383 bp nuclear genomic *Dnaaf2* locus (5′-ATCTAAGCCCCGTCGGTTAC-3′ and 5′-ACCGTGAAGGCTTAAGAGCA-3′), qPCR was performed on Stratagene Mx3005P using PerfeCTa SYBR Green SuperMix Low ROX (QuantaBio 95056) under the following conditions: 95°C for 2 min, 40 cycles of (95°C for 15 s, 60°C for 15 s, 72°C for 15 s, 80°C for 22 s), 60°C for 15 s and 95°C for 30 s.

ADP/ATP ratio measurement

The ADP/ATP ratio was determined using the ADP/ATP Ratio Assay Kit, Bioluminescent (Abcam, 65313) according to the manufacturer's instructions. In brief, freshly dissected embryos were placed in nucleotide-releasing buffer at one per well in a 96-well plate for 5 min. Reaction mix was added into each of the wells as per manufacturer's instructions. After 2 min incubation, luminescence from each well was measured using a POLARstar Omega microplate reader. Subsequently, ADP converting enzyme was added to each well. After 2 min incubation, luminescence from each well was measured as above. The ADP/ATP ratio was calculated following the manufacturer's instructions.

Imaging

Digital images of whole mount embryos were captured on a Nikon SMZ-1500 stereomicroscope equipped with a Spot Idea Digital Camera and Spot (v4.6) software. Images of sectioned embryos were taken with a Pannoramic MIDI slide scanner or Nikon Eclipse 50i equipped with a Spot Idea Digital Camera and Spot (v4.6) software or Nikon Eclipse Ti inverted microscope with an Andor Clara DR-1633 camera and Nikon NIS Elements AR software.

Quantification of phospho-Cdc25c (S216) foci

Immunofluorescent staining was used to identify the number of phospho-Cdc25c (S216) foci in mouse embryos. Total cells in each section were counted using both DAPI to mark nuclei and E-cadherin to mark cell membranes of epithelial cells. Counting was done using the multipoint tool in ImageJ. To calculate the ratio, the total number of phospho-Cdc25c (S216) foci was divided by the total number of e-cadherin- or DAPI-stained cells. The phospho-Cdc25c (S216) foci and total cell numbers were counted on every third section for each embryo analyzed.

Quantification of cells positive for actived caspase-3

Immunofluorescent staining with an antibody against cleaved caspase-3 was used to detect cells positive for active caspase-3. The total number of cells in each section were counted using DAPI to mark nuclei. Counting was done using the multipoint tool in ImageJ. To calculate the ratio, the total number of cleaved caspase-3 positive cells was divided by the total number of DAPI-stained cells. Cleaved caspase-3 positive cells and total cell numbers were counted on every third section for each embryo analyzed.

Statistical analysis

Statistical significance was analyzed using the Student's *t*-test (unpaired, two-tailed). Data shown in Fig. 5G, Fig. 6A and Fig. 7E are represented as mean±s.e.m.

Acknowledgements

We thank members of the Mager and Tremblay labs for providing useful input throughout the project. We thank the University of Massachusetts Medical School Core Electron Microscopy Facility for processing the mouse embryos for TEM and analyzing the data.

Competing interests

The authors declare no competing or financial interests.

Author contributions

Conceptualization: A.C., K.D.T., J.M.; Methodology: A.C., K.D.T., J.M.; Formal analysis: A.C., K.D.T., J.M.; Investigation: A.C., D.A., R.D., J.M.; Resources: E.I.; Data curation: A.C., D.A., R.D., E.I., J.M.; Writing - original draft: A.C., J.M.; Writing - review & editing: K.D.T., J.M.; Supervision: J.M.; Project administration: J.M.; Funding acquisition: J.M.

Funding

This work was supported by the National Institutes of Health (R01HD083311 to J.M.). Deposited in PMC for release after 12 months.

Peer review history

The peer review history is available online at https://dev.biologists.org/lookup/doi/10.1242/dev.188714.reviewer-comments.pdf

References

Babayev, E. and Seli, E. (2015). Oocyte mitochondrial function and reproduction. *Curr. Opin. Obstet. Gynecol.* **27**, 175-181. doi:10.1097/GCO.0000000000000164

Baker, C. N. and Ebert, S. N. (2013). Development of aerobic metabolism in utero: requirement for mitochondrial function during embryonic and fetal periods. *OA Biotechnology* **2**, 16. doi:10.13172/2052-0069-2-2-571

Barak, Y., Nelson, M. C., Ong, E. S., Jones, Y. Z., Ruiz-Lozano, P., Chien, K. R., Koder, A. and Evans, R. M. (1999). PPARγ is required for placental, cardiac, and adipose tissue development. *Mol. Cell* **4**, 585-595. doi:10.1016/S1097-2765(00)80209-9

Boengler, K., Heusch, G. and Schulz, R. (2011). Nuclear-encoded mitochondrial proteins and their role in cardioprotection. *Biochim. Biophys. Acta* **1813**, 1286-1294. doi:10.1016/j.bbamcr.2011.01.009

Bogenhagen, D. F., Ostermeyer-Fay, A. G., Haley, J. D. and Garcia-Diaz, M. (2018). Kinetics and mechanism of mammalian mitochondrial ribosome assembly. *Cell Rep.* **22**, 1935-1944. doi:10.1016/j.celrep.2018.01.066

Boonstra, J. and Post, J. A. (2004). Molecular events associated with reactive oxygen species and cell cycle progression in mammalian cells. *Genes* **337**, 1-13. doi:10.1016/j.gene.2004.04.032

Bult, C. J., Blake, J. A., Smith, C. L., Kadin, J. A., Richardson, J. E. and **The Mouse Genome Database Group**. (2019). Mouse Genome Database (MGD). *Nucleic Acids Res.* **47**, D801-D806. doi:10.1093/nar/gky1056

Bushdid, P. B., Osinska, H., Waclaw, R. R., Molkentin, J. D. and Yutzey, K. E. (2003). NFATc3 and NFATc4 are required for cardiac development and mitochondrial function. *Circ. Res.* **92**, 1305-1313. doi:10.1161/01.RES.0000077045.84609.9F

Camara, A. K. S., Zhou, Y., Wen, P.-C., Tajkhorshid, E. and Kwok, W.-M. (2017). Mitochondrial VDAC1: a key gatekeeper as potential therapeutic target. *Front. Physiol.* **8**, 460. doi:10.3389/fphys.2017.00460

Cerritelli, S. M., Frolova, E. G., Feng, C., Grinberg, A., Love, P. E. and Crouch, R. J. (2003). Failure to produce mitochondrial DNA results in embryonic lethality in Rnaseh1 null mice. *Mol. Cell* **11**, 807-815. doi:10.1016/S1097-2765(03)00088-1

Chandel, N. S. (2015). Evolution of mitochondria as signaling organelles. *Cell Metab.* **22**, 204-206. doi:10.1016/j.cmet.2015.05.013

Chen, H., Detmer, S. A., Ewald, A. J., Griffin, E. E., Fraser, S. E. and Chan, D. C. (2003). Mitofusins Mfn1 and Mfn2 coordinately regulate mitochondrial fusion and are essential for embryonic development. *J. Cell Biol.* **160**, 189-200. doi:10.1083/jcb.200211046

Clarke, P. R., Hoffmann, I., Draetta, G. and Karsenti, E. (1993). Dephosphorylation of cdc25-C by a Type-2A protein phosphatase: specific regulation during the cell cycle in xenopus egg extracts. *Mol. Biol. Cell* **4**, 397-411. doi:10.1091/mbc.4.4.397

Conrad, M., Jakupoglu, C., Moreno, S. G., Lippl, S., Banjac, A., Schneider, M., Beck, H., Hatzopoulos, A. K., Just, U., Sinowatz, F. et al. (2004). Essential role for mitochondrial thioredoxin reductase in hematopoiesis, heart development, and heart function. *Mol. Cell. Biol.* **24**, 9414-9423. doi:10.1128/MCB.24.21.9414-9423.2004

Crouch, S. P. M., Kozlowski, R., Slater, K. J. and Fletcher, J. (1993). The use of ATP bioluminescence as a measure of cell proliferation and cytotoxicity. *J. Immunol. Methods* **160**, 81-88. doi:10.1016/0022-1759(93)90011-U

Davies, V. J., Hollins, A. J., Piechota, M. J., Yip, W., Davies, J. R., White, K. E., Nicols, P. P., Boulton, M. E. and Votruba, M. (2007). Opa1 deficiency in a mouse model of autosomal dominant optic atrophy impairs mitochondrial morphology, optic nerve structure and visual function. *Hum. Mol. Genet.* **16**, 1307-1318. doi:10.1093/hmg/ddm079

De Silva, D., Tu, Y.-T., Amunts, A., Fontanesi, F. and Barrientos, A. (2015). Mitochondrial ribosome assembly in health and disease. *Cell Cycle* **14**, 2226-2250. doi:10.1080/15384101.2015.1053672

Dickinson, M. E., Flenniken, A. M., Ji, X., Teboul, L., Wong, M. D., White, J. K., Meehan, T. F., Weninger, W. J., Westerberg, H., Adissu, H. et al. (2016). High-throughput discovery of novel developmental phenotypes. *Nature* **537**, 508-514. doi:10.1038/nature19356

Dickinson, M. E., Flenniken, A. M., Ji, X., Teboul, L., Wong, M. D., White, J. K., Meehan, T. F., Weninger, W. J., Westerberg, H., Adissu, H., et al. (2017). High-throughput discovery of novel developmental phenotypes. *Nature* **551**, 398. doi:10.1038/nature24643

Downs, K. M. (2009). The enigmatic primitive streak: prevailing notions and challenges concerning the body axis of mammals. *BioEssays* **31**, 892-902. doi:10.1002/bies.200900038

Frei, C., Galloni, M., Hafen, E. and Edgar, B. A. (2005). The Drosophila mitochondrial ribosomal protein mRpL12 is required for Cyclin D/Cdk4-driven growth. *EMBO J.* **24**, 623-634. doi:10.1038/sj.emboj.7600523

Fu, W., Liu, Y. and Yin, H. (2019). Mitochondrial dynamics: biogenesis, fission, fusion, and mitophagy in the regulation of stem cell behaviors. *Stem Cells Int.* **2019**, 1-15. doi:10.1155/2019/9757201

Garg, S., Stölting, J., Zimorski, V., Rada, P., Tachezy, J., Martin, W. F. and Gould, S. B. (2015). Conservation of transit peptide-independent protein import into the mitochondrial and hydrogenosomal matrix. *Genome Biol. Evol.* **7**, 2716-2726. doi:10.1093/gbe/evv175

Goto, H., Yasui, Y., Nigg, E. A. and Inagaki, M. (2002). Aurora-B phosphorylates Histone H3 at serine28 with regard to the mitotic chromosome condensation. *Genes Cells* **7**, 11-17. doi:10.1046/j.1356-9597.2001.00498.x

Han, Y., Ishibashi, S., Iglesias-Gonzalez, J., Chen, Y., Love, N. R. and Amaya, E. (2018). Ca2+-induced mitochondrial ROS regulate the early embryonic cell cycle. *Cell Rep.* **22**, 218-231. doi:10.1016/j.celrep.2017.12.042

Hance, N., Ekstrand, M. I. and Trifunovic, A. (2005). Mitochondrial DNA polymerase gamma is essential for mammalian embryogenesis. *Hum. Mol. Genet.* **14**, 1775-1783. doi:10.1093/hmg/ddi184

Hendzel, M. J., Wei, Y., Mancini, M. A., Van Hooser, A., Ranalli, T., Brinkley, B. R., Bazett-Jones, D. P. and Allis, C. D. (1997). Mitosis-specific phosphorylation of histone H3 initiates primarily within pericentromeric heterochromatin during G2 and spreads in an ordered fashion coincident with mitotic chromosome condensation. *Chromosoma* **106**, 348-360. doi:10.1007/s004120050256

Herrmann, B. G., Labeit, S., Poustka, A., King, T. R. and Lehrach, H. (1990). Cloning of the T gene required in mesoderm formation in the mouse. *Nature* **343**, 617-622. doi:10.1038/343617a0

Hoffmann, I., Clarke, P. R., Marcote, M. J., Karsenti, E. and Draetta, G. (1993). Phosphorylation and activation of human cdc25-C by cdc2–cyclin B and its involvement in the self-amplification of MPF at mitosis. *EMBO J.* **12**, 53-63. doi:10.1002/j.1460-2075.1993.tb05631.x

Humble, M. M., Young, M. J., Foley, J. F., Pandiri, A. R., Travlos, G. S. and Copeland, W. C. (2013). Polg2 is essential for mammalian embryogenesis and is required for mtDNA maintenance. *Hum. Mol. Genet.* **22**, 1017-1025. doi:10.1093/hmg/dds506

Izumi, T. and Maller, J. L. (1993). Elimination of cdc2 Phosphorylation Sites in the cdc25 Phosphatase Blocks Initiation of M-Phase. *Mol. Biol. Cell* **4**, 1337-1350. doi:10.1091/mbc.4.12.1337

Jornayvaz, F. R. and Shulman, G. I. (2010). Regulation of mitochondrial biogenesis. *Essays Biochem.* **47**, 69-84. doi:10.1042/bse0470069

Kaneko, K. J. (2016). Metabolism of preimplantation embryo development: a bystander or an active participant? *Curr. Top. Dev. Biol.* **120**, 259-310. doi:10.1016/bs.ctdb.2016.04.010

Kim, H. R., Chae, H. J., Thomas, M., Miyazaki, T., Monosov, A., Monosov, E., Krajewska, M., Krajewski, S. and Reed, J. C. (2007). Mammalian dap3 is an essential gene required for mitochondrial homeostasis in vivo and contributing to the extrinsic pathway for apoptosis. *FASEB J.* **21**, 188-196. doi:10.1096/fj.06-6283com

Kumagai, A., Yakowec, P. S. and Dunphy, W. G. (1998). 14-3-3 proteins act as negative regulators of the mitotic inducer Cdc25 in Xenopus egg extracts. *Mol. Biol. Cell* **9**, 345-354. doi:10.1091/mbc.9.2.345

Kunji, E. R. S., Aleksandrova, A., King, M. S., Majd, H., Ashton, V. L., Cerson, E., Springett, R., Kibalchenko, M., Tavoulari, S., Crichton, P. G. et al. (2016). The transport mechanism of the mitochondrial ADP/ATP carrier. *Biochim. Biophys. Acta* **1863**, 2379-2393. doi:10.1016/j.bbamcr.2016.03.015

Larsson, N.-G., Wang, J., Wilhelmsson, H., Oldfors, A., Rustin, P., Lewandoski, M., Barsh, G. S. and Clayton, D. A. (1998). Mitochondrial transcription factor A is necessary for mtDNA maintenance and embryogenesis in mice. *Nat. Genet.* **18**, 231-236. doi:10.1038/ng0398-231

Lee, S. R. and Han, J. (2017). Mitochondrial nucleoid: shield and switch of the mitochondrial genome. *Oxidative Med. Cell. Longevity* **2017**, 8060949. doi:10.1155/2017/8060949

Li, P., Nijhawan, D., Budihardjo, I., Srinivasula, S. M., Ahmad, M., Alnemri, E. S. and Wang, X. (1997). Cytochrome c and dATP-dependent formation of Apaf-1/caspase-9 complex initiates an apoptotic protease cascade. *Cell* **91**, 479-489. doi:10.1016/S0092-8674(00)80434-1

Li, K., Li, Y., Shelton, J. M., Richardson, J. A., Spencer, E., Chen, Z. J., Wang, X. and Williams, R. S. (2000). Cytochrome c deficiency causes embryonic lethality and attenuates stress-induced apoptosis. *Cell* **101**, 389-399. doi:10.1016/S0092-8674(00)80849-1

Li, D. W., Yang, Q., Chen, J. T., Zhou, H., Liu, R. M. and Huang, X. T. (2005). Dynamic distribution of Ser-10 phosphorylated histone H3 in cytoplasm of MCF-7 and CHO cells during mitosis. *Cell Res.* **15**, 120-126. doi:10.1038/sj.cr.7290276

Lima, A., Burgstaller, J., Sanchez-Nieto, J. M. and Rodríguez, T. A. (2018). The mitochondria and the regulation of cell fitness during early mammalian development. *Curr. Top. Dev. Biol.* **128**, 339-363. doi:10.1016/bs.ctdb.2017.10.012

Liu, X., Kim, C. N., Yang, J., Jemmerson, R. and Wang, X. (1996). Induction of apoptotic program in cell-free extracts: requirement for dATP and cytochrome c. *Cell* **86**, 147-157. doi:10.1016/S0092-8674(00)80085-9

Liu, X.-M., Zhang, Y.-L., Ji, S.-Y., Zhao, L.-W., Shang, W.-N., Li, D., Chen, Z., Tong, C. and Fan, H.-Y. (2017). Mitochondrial function regulated by mitoguardin-1/2 is crucial for ovarian endocrine functions and ovulation. *Endocrinology* **158**, 3988-3999. doi:10.1210/en.2017-00487

Lodish, H., Berk, A., Zipursky, S. L., Matsudaira, P., Baltimore, D. and Darnell, J. (2000). Electron transport and oxidative phosphorylation. In *Molecular Cell Biology*, 4th edn. New York: W. H. Freeman and Company.

Mac Auley, A., Werb, Z. and Mirkes, P. E. (1993). Characterization of the unusually rapid cell cycles during rat gastrulation. *Development* **117**, 873-883.

Mishra, P. and Chan, D. C. (2014). Mitochondrial dynamics and inheritance during cell division, development and disease. *Nat. Rev. Mol. Cell. Biol.* **15**, 634-646. doi:10.1038/nrm3877
Ng, Y. S. and Turnbull, D. M. (2016). Mitochondrial disease: genetics and management. *J. Neurol.* **263**, 179-191. doi:10.1007/s00415-015-7884-3
Nonn, L., Williams, R. R., Erickson, R. P. and Powis, G. (2003). The absence of mitochondrial thioredoxin 2 causes massive apoptosis, exencephaly, and early embryonic lethality in homozygous mice. *Mol. Cell. Biol.* **23**, 916-922. doi:10.1128/MCB.23.3.916-922.2003
O'Brien, T. W., Liu, J., Sylvester, J. E., Mougey, E. B., Fischel-Ghodsian, N., Thiede, B., Wittmann-Liebold, B. and Graack, H.-R. (2000). Mammalian mitochondrial ribosomal proteins (4). *J. Biol. Chem.* **275**, 18153-18159. doi:10.1074/jbc.M909762199
O'Connor, C. (2008). Cell division: stages of mitosis. *Nat. Educ.* **1**, 188.
Park, C. B., Asin-Cayuela, J., Cámara, Y., Shi, Y., Pellegrini, M., Gaspari, M., Wibom, R., Hultenby, K., Erdjument-Bromage, H., Tempst, P. et al. (2007). MTERF3 is a negative regulator of mammalian mtDNA transcription. *Cell* **130**, 273-285. doi:10.1016/j.cell.2007.05.046
Peng, C.-Y., Graves, P. R., Thoma, R. S., Wu, Z., Shaw, A. S. and Piwnica-Worms, H. (1997). Mitotic and G2 checkpoint control: regulation of 14-3-3 protein binding by phosphorylation of Cdc25C on serine-216. *Science* **277**, 1501-1505. doi:10.1126/science.277.5331.1501
Peng, C. Y., Graves, P. R., Ogg, S., Thoma, R. S., Byrnes, M. J., Wu, Z., Stephenson, M. T. and Piwnica-Worms, H. (1998). C-TAK1 protein kinase phosphorylates human Cdc25C on serine 216 and promotes 14-3-3 protein binding. *Cell Growth Differ.* **9**, 197-208.
Piruat, J. I., Pintado, C. O., Ortega-Saenz, P., Roche, M. and Lopez-Barneo, J. (2004). The mitochondrial SDHD gene is required for early embryogenesis, and its partial deficiency results in persistent carotid body glomus cell activation with full responsiveness to hypoxia. *Mol. Cell. Biol.* **24**, 10933-10940. doi:10.1128/MCB.24.24.10933-10940.2004
Power, M.-A. and Tam, P. P. L. (1993). Onset of gastrulation, morphogenesis and somitogenesis in mouse embryos displaying compensatory growth. *Anat. Embryol.* **187**, 493-504. doi:10.1007/BF00174425
Prigione, A., Ruiz-Pérez, M. V., Bukowiecki, R. and Adjaye, J. (2015). Metabolic restructuring and cell fate conversion. *Cell. Mol. Life Sci.* **72**, 1759-1777. doi:10.1007/s00018-015-1834-1
Qian, J., Colbert, M. C., Witte, D., Kuan, C.-Y., Gruenstein, E., Osinska, H., Lanske, B., Kronenberg, H. M. and Clemens, T. L. (2003). Midgestational lethality in mice lacking the parathyroid hormone (PTH)/PTH-related peptide receptor is associated with abrupt cardiomyocyte death. *Endocrinology* **144**, 1053-1061. doi:10.1210/en.2002-220993
Ratnaparkhi, A. (2013). Signaling by Folded gastrulation is modulated by mitochondrial fusion and fission. *J. Cell Sci.* **126**, 5369-5376. doi:10.1242/jcs.127985
Robles, P. and Quesada, V. (2017). Emerging roles of mitochondrial ribosomal proteins in plant development. *Int. J. Mol. Sci.* **18**, 2595. doi:10.3390/ijms18122595
Rojansky, R., Cha, M.-Y. and Chan, D. C. (2016). Elimination of paternal mitochondria in mouse embryos occurs through autophagic degradation dependent on PARKIN and MUL1. *eLife* **2016**, e17896. doi:10.7554/eLife.17896.016
Roshak, A. K., Capper, E. A., Imburgia, C., Fornwald, J., Scott, G. and Marshall, L. A. (2000). The human polo-like kinase, PLK, regulates cdc2/cyclin B through phosphorylation and activation of the cdc25C phosphatase. *Cell. Signal.* **12**, 405-411. doi:10.1016/S0898-6568(00)00080-2
Schaefer, A., Lim, A. and Gorman, G. (2019). Epidemiology of mitochondrial disease. In *Diagnosis and Management of Mitochondrial Disorders* (ed. M. Mancuso and T. Klopstock). pp. 63-79. Cham: Springer.
Schatten, H., Sun, Q.-Y. and Prather, R. (2014). The impact of mitochondrial function/dysfunction on IVF and new treatment possibilities for infertility. *Reprod. Biol. Endocrinol.* **12**, 111. doi:10.1186/1477-7827-12-111
Schöler, H. R., Dressler, G. R., Balling, R., Rohdewohld, H. and Gruss, P. (1990). Oct-4: a germline-specific transcription factor mapping to the mouse t-complex. *EMBO J.* **9**, 2185-2195. doi:10.1002/j.1460-2075.1990.tb07388.x
Snow, M. H. L. (1977). Gastrulation in the mouse: growth and regionalization of the epiblast. *Development* **42**, 293-303.
Steenbergen, R., Nanowski, T. S., Beigneux, A., Kulinski, A., Young, S. G. and Vance, J. E. (2005). Disruption of the phosphatidylserine decarboxylase gene in mice causes embryonic lethality and mitochondrial defects. *J. Biol. Chem.* **280**, 40032-40040. doi:10.1074/jbc.M506510200
Strausfeld, U., Fernandez, A., Capony, J.-P., Girard, F., Lautredou, N., Derancourt, J., Labbe, J.-C. and Lamb, N. J. (1994). Activation of p34cdc2 protein kinase by microinjection of human cdc25C into mammalian cells. *J. Biol. Chem.* **269**, 5989-6000.
Sun, M. G., Williams, J., Munoz-Pinedo, C., Perkins, G. A., Brown, J. M., Ellisman, M. H., Green, D. R. and Frey, T. G. (2007). Correlated three-dimensional light and electron microscopy reveals transformation of mitochondria during apoptosis. *Nat. Cell Biol.* **9**, 1057-1065. doi:10.1038/ncb1630
Tait, S. W. G. and Green, D. R. (2012). Mitochondria and cell signalling. *J. Cell Sci.* **125**, 807-815. doi:10.1242/jcs.099234
Tremblay, K. D., Dunn, N. R. and Robertson, E. J. (2001). Mouse embryos lacking Smad1 signals display defects in extra-embryonic tissues and germ cell formation. *Development* **128**, 3609-3621.
Wakabayashi, J., Zhang, Z., Wakabayashi, N., Tamura, Y., Fukaya, M., Kensler, T. W., Iijima, M. and Sesaki, H. (2009). The dynamin-related GTPase Drp1 is required for embryonic and brain development in mice. *J. Cell Biol.* **186**, 805-816. doi:10.1083/jcb.200903065
Wei, Y., Mizzen, C. A., Cook, R. G., Gorovsky, M. A. and Allis, C. D. (1998). Phosphorylation of histone H3 at serine 10 is correlated with chromosome condensation during mitosis and meiosis in Tetrahymena. *Proc. Natl. Acad. Sci. USA* **95**, 7480-7484. doi:10.1073/pnas.95.13.7480
Wilkinson, D. G., Bhatt, S. and Herrmann, B. G. (1990). Expression pattern of the mouse T gene and its role in mesoderm formation. *Nature* **343**, 657-659. doi:10.1038/343657a0
Yagi, M., Uchiumi, T., Takazaki, S., Okuno, B., Nomura, M., Yoshida, S.-I., Kanki, T. and Kang, D. (2012). p32/gC1qR is indispensable for fetal development and mitochondrial translation: importance of its RNA-binding ability. *Nucleic Acids Res.* **40**, 9717-9737. doi:10.1093/nar/gks774
Yamaguchi, R. and Perkins, G. (2009). Dynamics of mitochondrial structure during apoptosis and the enigma of Opa1. *Biochim. Biophys. Acta.* **1787**, 963-972. doi:10.1016/j.bbabio.2009.02.005
Yao, C.-H., Wang, R., Wang, Y., Kung, C.-P., Weber, J. D. and Patti, G. J. (2019). Mitochondrial fusion supports increased oxidative phosphorylation during cell proliferation. *eLife* **8**, e41351. doi:10.7554/eLife.41351
Yates, B., Braschi, B., Gray, K. A., Seal, R. L., Tweedie, S. and Bruford, E. A. (2017). Genenames.org: the HGNC and VGNC resources in 2017. *Nucleic Acids Res.* **45**, D619-D625. doi:10.1093/nar/gkw1033
Youle, R. J. and van der Bliek, A. M. (2012). Mitochondrial fission, fusion, and stress. *Science* **337**, 1062-1065. doi:10.1126/science.1219855
Zhang, J., Wang, X., Vikash, V., Ye, Q., Wu, D., Liu, Y. and Dong, W. (2016). ROS and ROS-mediated cellular signaling. *Oxidative Med. Cell. Longevity* **2016**, 4350965. doi:10.1155/2016/4350965
Zhang, D., Keilty, D., Zhang, Z.-F. and Chian, R.-C. (2017). Mitochondria in oocyte aging: current understanding. *Facts, Views Vison obGyn* **9**, 29-38.
Zhong, H. and Yin, H. (2015). Role of lipid peroxidation derived 4-hydroxynonenal (4-HNE) in cancer: focusing on mitochondria. *Redox Biol.* **4**, 193-199. doi:10.1016/j.redox.2014.12.011

Summary: Knockout of any one of 19 different mitochondrial ribosomal protein genes results in failure to initiate gastrulation, suggesting that distinct energy systems are crucial at specific times during mammalian development.

Funding details

S.No.	Funder name	Funder ID	Grant ID
1	National Institutes of Health	http://dx.doi.org/10.13039/100000002	R01HD083311